A Thesis

entitled

An Investigation of Force and Vibration Transmission Characteristic of Power Circulatory Four Square Type Gear Test Machines

by

Mehmet Seha Tatlier

Submitted as partial fulfillment of the requirements for

the *Master of Science* in *Mechanical Engineering*

_____

Dr Ahmet Kahraman

_____

Dr Ali Fatemi

_____

Dr Cedric Mousseau

_____

Graduate School

The University of Toledo

December 2002

An abstract of

An Investigation of Force and Vibration Transmission Characteristic of Power Circulatory Four Square Type Gear Test Machines

Mehmet Seha Tatlier

Submitted as partial fulfillment of the requirements for

the *Master of Science* in *Mechanical Engineering*

The University of Toledo

December 2002

In this study, two types of dynamic models are developed to investigate the dynamic behavior of four-square gear test machines. The first model is based on three-dimensional finite elements of the shafts connecting the test and reaction gearboxes, combined with three-dimensional stiffness models of helical gear pairs and rolling element bearings. The second model represents a limiting case when only torsional motions are allowed. The gear transmission errors and eccentricities are considered as the excitations for both models. Eigen Value solution and Modal Summation Technique are used to compute natural modes and forced response, respectively.

A number of gear dynamics and durability test machines are considered as the example cases. The interactions between the test and reaction gearboxes are investigated for each test machine to determine their force and vibration isolation capabilities. The

effect of any added torsional flexibility or rigid inertia between the test and reaction gear sets on the isolation of the test gear pair from the disturbances originated at the reaction gearbox are studied. At the end, the torsional model is used to derive simplified equations that can potentially be used for designing such machines with acceptable vibration isolation characteristics. With the help of these equations, a designer can select the required flexibility for the connecting shafts.

ACKNOWLEDGEMENTS

I would like to extend sincere thanks to my advisor, Dr Ahmet Kahraman, for his continuous support and guidance during the course of this study. He has been a constant inspiration and guiding force behind the completion of this research work. I am thankful to him for all the expertise and knowledge he has shared with me.

I wish to express my gratitude Dr Ali Fatemi and Dr Cedric Mousseau for kindly agreeing to serve on the thesis defense committee.

Finally, I would like to thank all my colleagues in the CGR lab for their help and support during this research work.

TABLE OF CONTENTS

LIST OF FIGURES

LIST OF TABLES

CHAPTER 1

INTRODUCTION

1.1 Background Motivation

Gears are used commonly in almost every industrial application including automotive, aerospace, machine tool and marine industries. Gears offer an efficient and reliable means of torque/power and motion transfer. As gear systems are operated under diverse conditions, their functionality becomes closely linked to the functionality of the overall system. For instance, gears used in an automotive transmission must endure severe duty cycles for the transmission to be functional under the different conditions. Similarly, the operation of the gears must be quiet such that lower overall noise levels can be achieved for the transmission.

While significant amount of modeling studies were performed on the dynamics and durability of gear systems to quantify and improve on noise and fatigue life characteristics, due to the complexity of the real life systems and a large number of parameters involved, the need for actual gear experiments could not be eliminated. It is still common practice to evaluate gears for dynamics and durability through experimental methods. Such experimental studies also provide the data required to validate the simulation models.

There are two different gear test machine concepts that have been used commonly in the past. The layouts of these machine concepts are shown in Figure 1.1. The first type in Figure 1.1(a) is an open-end type gear test machine. A gear pair located in the middle is powered by a motor at one end. The power is transmitted through the gear pair to the other end and absorbed by a brake (load) dynamometer. In this arrangement, gears can be operated at any desired speed and torque conditions. This allows a simulation of actual duty cycles at varying torque and speed values provided that the controller is capable of doing so. The arrangement is general such that gears or transmissions requiring different center distances can be accommodated using open-end test machines. Meanwhile as all the required power must be generated by the electric motor in real time, the requirements for power/torque capacity is often large resulting in very large fixed dynamometer facilities. In addition, a precise control of the speed and torque require an expensive control unit. In spite of these disadvantages, open-end test machines have been used very commonly for both durability and dynamics evaluations of gear systems. For instance, Iida, et. al. [1] employed an open-end test machine to investigate the effects of geometrical eccentricity and unbalance of a gear on the free and forced vibration of a shaft in a spur geared system. They [2] later included another study on how the friction force between gear under mixed and boundary lubrication influences the vibrational system. Umezawa and Sato [3] studied the influence of numerous gear errors including pitch errors and pressure angle errors on the vibration levels of a profile corrected spur gear pair. They also [4] performed a study on the vibration and noise problems of the helical gear pair with a narrow facewidth. The same open-end test machine was used later to estimate the vibrational behavior of gears enclosed in a gear case by measuring the

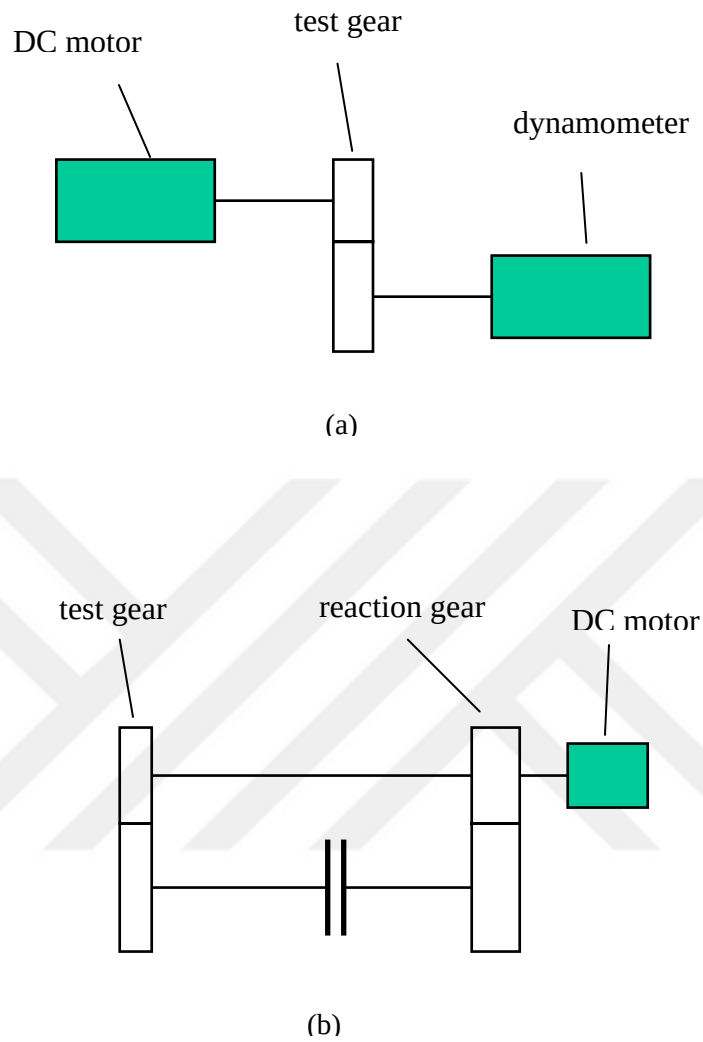

Figure 1.1(a) Open-end type testing machine (b) Power circulatory four-square type testing machine.

exterior vibrations [5]. Choy and Ruan [6] compared experimental results of vibration, dynamic load, and noise data of geared transmission collected from an open-end test machine with analytical methods. Finally Liou, et. al. [7] performed a study on the effect of contact ratio on dynamic loads of spur gear pairs.

The other type of test machines is *power-circulatory four-square* type arrangement as shown in Figure 1.1(b). In this case, two gear pairs of the same center distance and gear ratio are coupled to each other through connecting shafts. A constant torque is applied to this closed loop through either hydraulic actuators or split couplings. A small DC motor connected to one of the shafts is used to overcome mechanical losses in order to operate the system at the desired rotational speeds. Four-square type gear testing machines are compact since the DC motor capacity is relatively small. This makes these machines significantly more compact that the open-end machines. Operation of gears under a constant torque is a definite advantage of these machines as the controller is reduced to a simple speed controller. However, these machines are not as versatile as open-end machines since the center distances and the gear ratios are fixed. They also cannot be operated as conveniently as open-end test machines under variable torque, duty cycle conditions. However, their advantages overweigh their disadvantages in most applications making them the layout of the choice for many durability and dynamic gear tests.

On the durability side, Townsend and colleagues [8-11] used the four-square machine shown in Figure 1.2 to study the influence of gear materials, surface treatments and synthetic lubricants on pitting fatigue life of spur gears. Yoshida, et. al. [12] used power circulatory gear testing machine in order to elucidate the failure mode, load

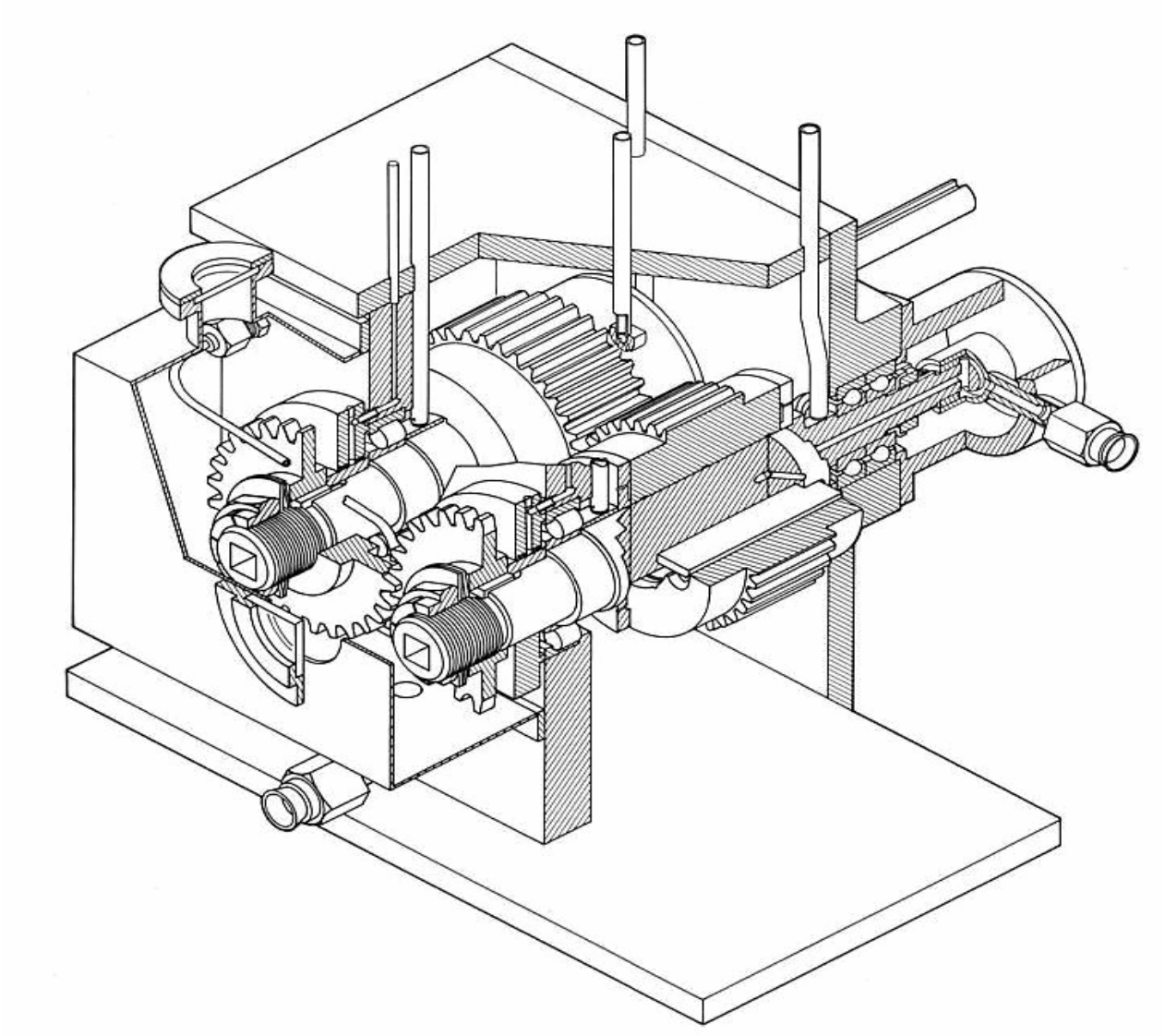

Figure 1.2. NASA gear durability test machine.

carrying capacity and relationship between tooth profile change and dynamic performance. Yamanaka, et. al. [13] performed tests to quantify the pitting life of carburized gears as a function of the type of lubrication including automatic transmission fluid and traction oil. Similarly Dahmen, and Schonwerth [14] investigated the influence of lubricant additives on gear contact load carrying capacity. Schaller, et. al. [15] studied on strength investigation for pit forming on hardened gear flank with using the FZG machine shown in Figure 1.3.

On the other hand power circulatory four-square machines are also used for dynamic tests by many researchers. Harris [16] studied modes of vibration of four-square machines. Munro [17] used a four-square machine to study the dynamic behavior of spur gears in experimentally. Later he investigated [18] the effect of the profile relief on the transmission error characteristic of spur and helical gears, under both static and dynamic conditions. Utagawa and Harada [19] compared measured results of dynamic loads on spur gear teeth with calculated results on high speed testing machine. Gregory, et. al.[20] employed the Munro's machine to estimate the dynamic load for various damping values. Nakamura [21] used a four-square test machine in an anechoic room to describe the effect the dynamic gear and bearing loads on gear noise. Seager [22] performed an experimental study of torsional and transverse motions of a pair of helical gears. Remmers [23] studied the effects resultant dynamic forces from the interaction between gear tooth errors and combined mass-inertia-elastic characteristic of complete gear system. Ichimaru and Hirano [24] interaction between tooth deformation and dynamic load and investigated the effects on the fatigue failure. Kiyono, et. al. [25] investigated the dynamic behaviors of helical gears through measurements of acceleration levels in a

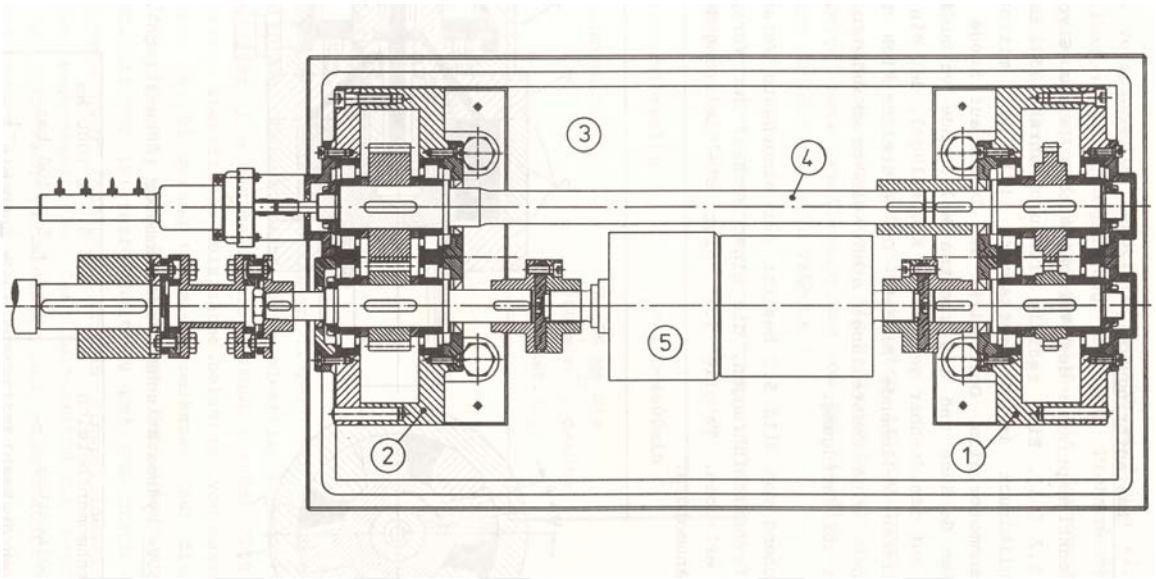

Figure 1.3 FZG gear test machine.

four-square test machine. Kahraman and Blankenship [26-30] performed experiments on nonlinear dynamic behavior of spur gear pair using a high-speed four-square test machine shown in Figure 1.4. Their investigation included the influence of gear mesh parameters such as involute contact ratio and gear tooth modifications. Later Wagaj and Kahraman [31] utilized the same machine to validate quasi-static motion transfer error predictions of a gear contact analysis model.

As the literature is searched there is hardly any study about the design of these machines. Previous studies are mostly about the usage of these machines. For this reason, this study is about the design of these machines.

While power-circulatory four-square test machines offer a convenient way to test parallel axis gear pairs, there are major issues associated with the accuracy of the data collected. As mentioned earlier, two gear sets, a *test gear pair* and a *reaction gear pair*, must be connected to each other to form a closed loop. The goal here is to measure the fatigue life or the dynamic behavior (dynamic stresses, dynamic motion transmission error or dynamic bearing vibrations) of the test gear pair accurately. Yet, the reaction gear pair that operates at the same speed and torque values creates dynamic forces and motion transfer errors as well. These disturbances can potentially travel to the test gear pair to corrupt the dynamic or fatigue behavior of the test gear pair. In other words, the interaction of test and reaction gear pairs is a major issue in four-square machine design. Several practical guidelines have been used in the past to improve the isolation of the test gear pair from the reaction gear pair including the following:

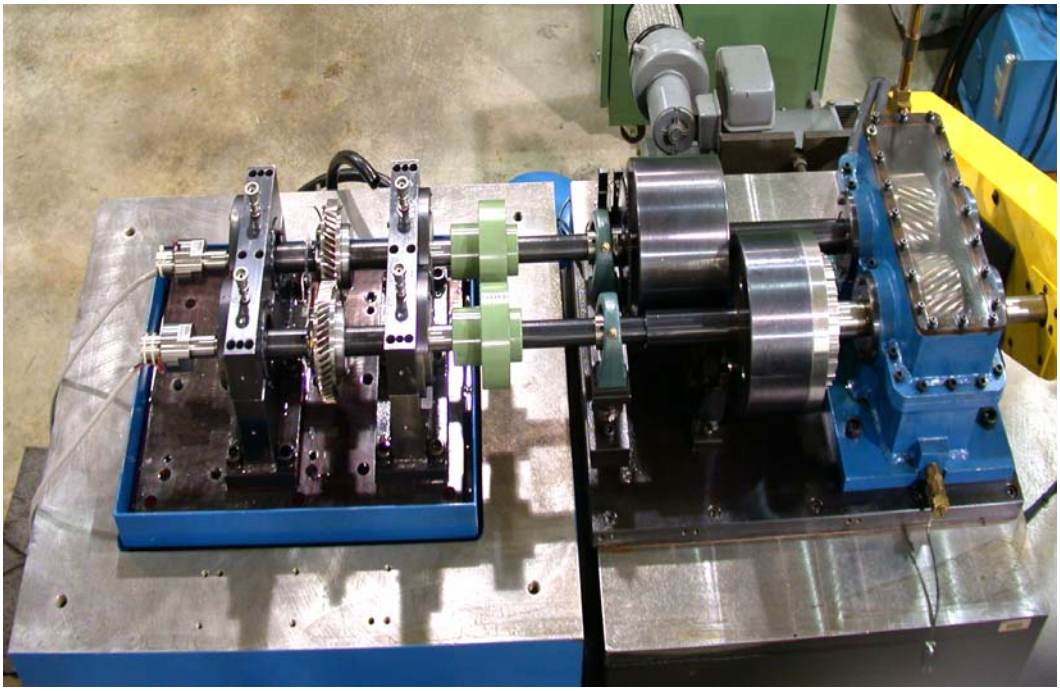

Figure 1.4 Gear dynamic test machine.

- Minimize the dynamic excitations caused by the reaction gear set by using high-precision, high-contact-ratio gear helical gears as reaction gears.
- Use flexible shafts with flywheels for connecting the two gear pair to serve as a mechanical filter isolating the disturbances coming from the reaction gear pair. Use of flexible couplings that are very compliant in torsion can also be included here.
- Use a different numbers of teeth for the reaction gears and the test gears such that the fundamental gear mesh frequencies and their harmonics are distinct. This way any disturbances traveled to the test gear side from the reaction gear side can be identified easily.

While these design guidelines can be made work to have an acceptable level of vibration isolation, a dynamic model of the overall system is required to quantify many of the above parameters and predict the effectiveness of these measures. For instance, questions including how flexible the shafts must be, how large and at which location the flywheel inertias must be designed, and how much flexibility is needed from couplings can only be answered by a detailed dynamic model. In addition, other dynamic characteristics are also of particular interest. For instance while shafts are made long and slender to address the isolation issue, they will have their own dynamics problems in the form of flexural vibrations. A dynamic model can be used to not only identify such adverse side affects of the above design measures but also to bring solutions to these effects. Such a dynamic model of power-circulatory four-square test machines is the main motivation behind this study.

1.2 Scope and Objectives

The main objective of this study is to arrive at guidelines for design of four-square test machines with acceptable isolation characteristics under dynamic conditions. Any disturbances originated at the reaction gear mesh might potentially travel to the test gearbox, altering the dynamic loading conditions of the test gear mesh, and hence, influencing the outcome of the durability or dynamics test. Therefore, a proper design of connecting structures becomes a major priority. In order to achieve the above goal, a general three-dimensional dynamic model of four-square test machines will be developed in this study. Also purely torsional dynamic model will be developed to investigate dynamic characteristics. A number of most popular four-square test machines like the ones shown in Figures 1.2 to 1.4 will be used to demonstrate the capabilities of the models. Extensive parametric studies will be performed at the end to derive easy-to-use guidelines for design of four-square test machines with acceptable performance characteristics

1.3 Thesis Outline

A detailed formulation of the three-dimensional model and a limited case of a torsional model is given in Chapter 2. The example systems of four-square type gear dynamic machines used to demonstrate the capabilities of the models is discussed in

Chapter 3. Finally, the simple design guidelines for the design of four-square test machines are listed in Chapter 4.

CHAPTER 2

DYNAMIC MODELS

2.1 Three Dimensional Dynamic Model

2.1.1 Model Capabilities and Assumptions

The three dimensional dynamic model will be capable of predicting transverse vibrations such as bearing vibrations and shaft bending vibrations whereas the torsional model, which will be proposed in the next section should be sufficient for predicting the torsional natural modes and for investigating the vibration transmission/isolation issues. Such motions should become important especially when the shafts connecting the test and reaction gear sets are made more flexible. In this section, a transverse-torsional model of the system shown in Figure 1.1(b) will be developed. The model will be based on a general formulation to analyze any two shafts connected to each other through two separate gear meshes. This general model is to have the following capabilities:

- The model should include transverse, torsional, axial and rotational (bending) motions of the gear pairs that can be of spur or helical type.
- The model should be capable of simulating any shaft geometries including variable cross-sections, and the hollow shafts. The shaft transverse, torsional, axial and bending motions should all be included in the model.

- Any couplings, flywheels and rigid inertias that are mounted on the shafts including the rotatory inertia of the DC motor can be included.
- The model should have the ability to included any number of rolling element bearings of any type supporting the shafts at specified locations positioned at any location on the shafts

A number of assumptions will be made in developing the 3D model. As gears rotate, number of tooth pairs in each gear mesh fluctuates between two integer values, typically between 1 and 2. This results in a time-varying gear mesh stiffness causing parametric instabilities at twice the resonance frequencies. As such parametric resonance frequencies are quite large, mesh stiffness fluctuations will be neglected here. Also gears are subjected to certain amount of backlash at the mesh. If the vibration amplitudes are excessive such that tooth separations can happen, a nonlinear model is needed for the simulation. In this study, it is assumed that tooth separations do not occur such that a linear model is sufficient.

This model will be obtained by expanding an already existing geared rotor dynamics model [32]. This model was developed to study the coupled spur gear-shaft-bearing dynamics of a two-shaft, single-gear pair system and later expanded to include three shaft gear reduction units [33]. A lumped- parameter model of gear pair was combined with a finite element model of the shafts to predict the natural modes and the forced response due to static transmission error excitation. This model will be modified to include axial and bending motions of the shafts and gears to include helical gears, and a second gear pair coupling will be added to obtain the model of any four-square type arrangement.

The model will be made general such that any system of the same layout can be analyzed to allow parametric design optimization studies. In the following sections, the model formulation will be outlined. Only the essential details will be given here as further details can be found in references [32,33].

2.1.2 The Shaft Model

The general system shown in Figure 1.1(b) has two parallel-axis shafts connected to each other at two places through spur or helical gears. Finite element model of each shaft can be developed by using Euler-Bernoelli beam elements [34]. Considering a finite element ℓ on one of the shafts defined by two nodes ℓ and $\ell+1$ as shown in Figure 2.1, the stiffness and mass/inertia matrices of this ℓ-th shaft (rotor) element are given as a summation of bending, torsion and axial components as

$$\mathbf{k}_{s\ell} = (\mathbf{k}_{s\ell})_{bending} + (\mathbf{k}_{s\ell})_{torsion} + (\mathbf{k}_{s\ell})_{axial}, \tag{2.1}$$

$$\mathbf{m}_{s\ell} = (\mathbf{m}_{s\ell})_{bending+axial} + (\mathbf{m}_{s\ell})_{rotation} + (\mathbf{m}_{s\ell})_{torsion} \tag{2.2}$$

where the individual components of $\mathbf{k}_{s\ell}$ and $\mathbf{m}_{s\ell}$ are given in Reference [33]. These shaft element matrices of dimension 12 can be put into the form

$$\mathbf{k}_{s\ell} = \begin{bmatrix} (\mathbf{k}_{11})_\ell & (\mathbf{k}_{21})_\ell^T \\ (\mathbf{k}_{21})_\ell & (\mathbf{k}_{22})_\ell \end{bmatrix}, \qquad \mathbf{m}_{s\ell} = \begin{bmatrix} (\mathbf{m}_{11})_\ell & (\mathbf{m}_{21})_\ell^T \\ (\mathbf{m}_{21})_\ell & (\mathbf{m}_{22})_\ell \end{bmatrix} \tag{2.3,4}$$

.

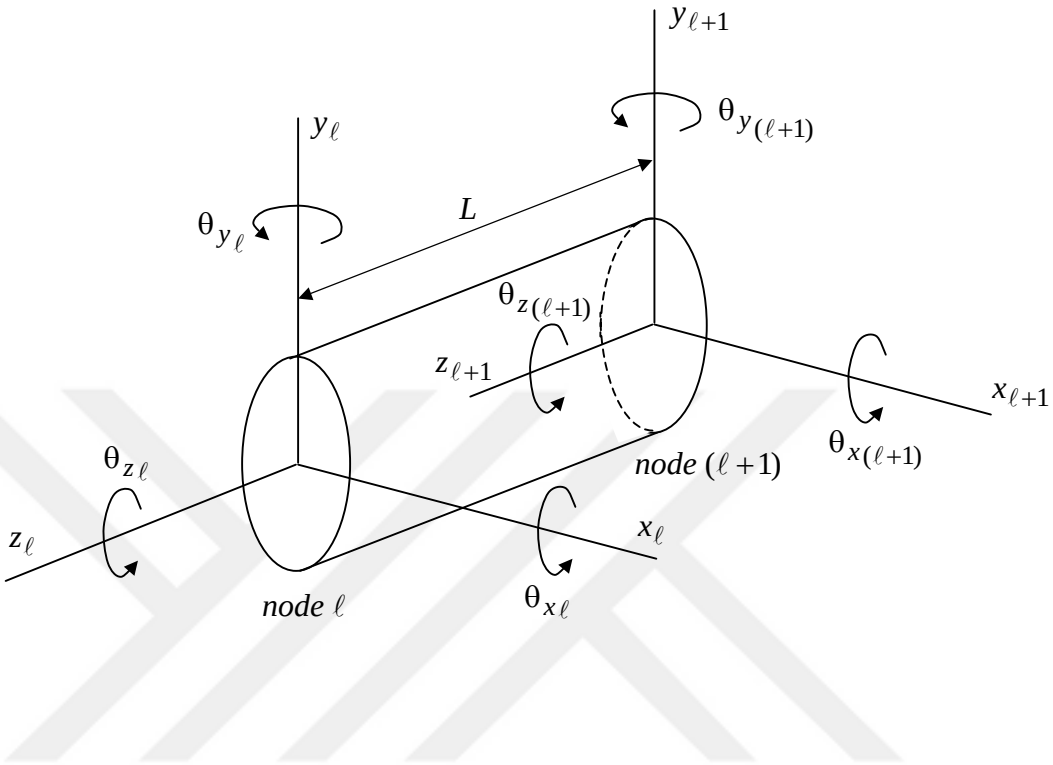

Figure 2.1 A finite shaft (rotor) element [34].

Starting with the first shaft, if the shaft is defined by m_1 finite rotor elements ($\ell = 1, 2, \ldots, m_1$), the stiffness and mass matrices of the entire shaft 1 can be assembled as:

$$\mathbf{K}_{s1} = \begin{bmatrix} (\mathbf{k}_{11})_1 & & & & \textit{symmetric} & \\ (\mathbf{k}_{21})_1 & (\mathbf{k}_{22})_1 + (\mathbf{k}_{11})_2 & & & & \\ \mathbf{0} & (\mathbf{k}_{21})_2 & (\mathbf{k}_{22})_2 + (\mathbf{k}_{11})_3 & & & \\ \vdots & \vdots & \vdots & \ddots & & \\ \mathbf{0} & \mathbf{0} & \mathbf{0} & \cdots & (\mathbf{k}_{22})_{(m_1-1)} + (\mathbf{k}_{11})_{m_1} & \\ \mathbf{0} & \mathbf{0} & \mathbf{0} & \cdots & (\mathbf{k}_{21})_{m_1} & (\mathbf{k}_{22})_{m_1} \end{bmatrix} \tag{2.5}$$

$$\mathbf{M}_{s1} = \begin{bmatrix} (\mathbf{m}_{11})_1 & & & & \textit{symmetric} & \\ (\mathbf{m}_{21})_1 & (\mathbf{m}_{22})_1 + (\mathbf{m}_{11})_2 & & & & \\ \mathbf{0} & (\mathbf{m}_{21})_2 & (\mathbf{m}_{22})_2 + (\mathbf{m}_{11})_3 & & & \\ \vdots & \vdots & \vdots & \ddots & & \\ \mathbf{0} & \mathbf{0} & \mathbf{0} & \cdots & (\mathbf{m}_{22})_{(m_1-1)} + (\mathbf{m}_{11})_{m_1} & \\ \mathbf{0} & \mathbf{0} & \mathbf{0} & \cdots & (\mathbf{m}_{21})_{m_1} & (\mathbf{m}_{22})_{m_1} \end{bmatrix} \tag{2.6}$$

The above formulation is applied to the second shaft that is described by a total of m_2 finite elements to obtain $\mathbf{K}_{s2}$ and $\mathbf{M}_{s2}$. The overall shaft stiffness $\mathbf{K}_s$ and mass $\mathbf{M}_s$ matrices are then assembled as

$$\mathbf{K}_s = \begin{bmatrix} \mathbf{K}_{s1} & \mathbf{0} \\ \mathbf{0} & \mathbf{K}_{s2} \end{bmatrix}, \qquad \mathbf{M}_s = \begin{bmatrix} \mathbf{M}_{s1} & \mathbf{0} \\ \mathbf{0} & \mathbf{M}_{s2} \end{bmatrix} \tag{2.7}$$

Both $\mathbf{K}_s$ and $\mathbf{M}_s$ are square matrices of dimension S where the total number of degrees of freedom is $S = 6(m_1 + m_2 + 2)$.

2.1.3 Gear System Matrices

A three-dimensional dynamic model of helical gear pair is shown in Figure 2.2 will be employed here [33, 35]. The test gear pair is chosen as the example for this formulation formed by gears *t*1 and *t*2. Both gears are assumed to have rigid blanks that are connected to each other by a linear gear mesh spring $\bar{k}_t$ on the plane of action in the tooth normal direction determined by the helix angle β_t. Also applied in the same direction connected in series to $\bar{k}_t$ is a displacement excitation in the form motion transmission error $e_t(t)$. The relative positions of the gears are such that the line connecting the gear centers forms the positive *x*-axis of the coordinate frame. In this position, the plane of action makes an angle ψ_t with the positive *y*-axis as shown in Figure 2.2. As the plane of action changes direction depending on the direction of the loading, ψ_t is defined as

$$\psi_t = \begin{cases} \phi_t, & T_{t1} : counter\ clockwise \\ -\phi_t, & T_{t1} : clockwise \end{cases} \tag{2.8}$$

where ϕ_t is the transverse pressure angle of the gear pair and T_{t1} is the torque applied on the test gear *t*1. Helix angle β_t is defined based on the hand of the gear *t*1 as

$$\beta_t = \begin{cases} (+)ve & if\ \ gear\ t1\ has\ \ left\ hand\ \ teeth \\ (-)ve & if\ \ gear\ t1\ has\ \ right\ \ hand\ \ teeth \end{cases} \tag{2.9}$$

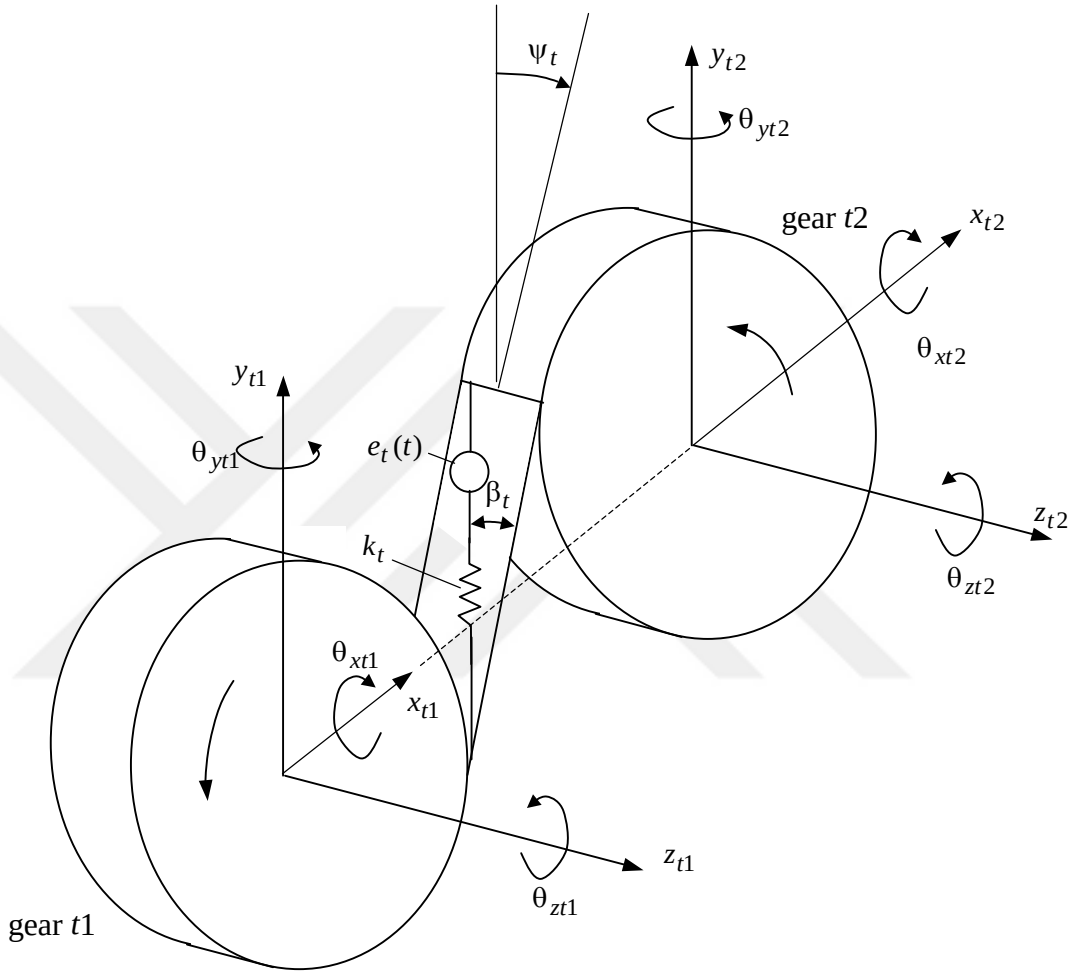

Figure 2.2. A 3D dynamic model of a helical gear pair [33, 35].

Both gears are allowed to translate in *x* and *y* directions in the transverse plane and in the axial *z* direction. In addition, each gear is allowed to rotate about these three axes by θ_x, θ_y and θ_z, respectively. Hence, with six degrees of freedom on each gear, the gear pair *t* has a total of 12 degrees of freedom that defines the coupling between the two shafts holding the gears. Equations of motion for gear *t*1 are given as:

$$m_{t1}\ddot{y}_{t1} + c_t\dot{p}_t(t) + \bar{k}_t p_t(t)\cos\beta_t\cos\psi_t = 0 \qquad \text{(2.10a-f)}$$

$$m_{t1}\ddot{x}_{t1} + c_t\dot{p}_t(t) + \bar{k}_t p_t(t)\cos\beta_t\sin\psi_t = 0$$

$$m_{t1}\ddot{z}_{t1} - c_t\dot{p}_t(t) - \bar{k}_t p_t(t)\sin\beta_t = 0$$

$$I_{t1}\ddot{\theta}_{yt1} + r_{t1}c_t\dot{p}_t(t) + r_{t1}\bar{k}_t p_t(t)\sin\beta_t\cos\psi_t = 0$$

$$I_{t1}\ddot{\theta}_{xt1} + r_{t1}c_t\dot{p}_t(t) + r_{t1}\bar{k}_t p_t(t)\sin\beta_t\sin\psi_t = 0$$

$$J_{t1}\ddot{\theta}_{zt1} + r_{t1}c_t\dot{p}_t(t) + r_{t1}\bar{k}_t p_t(t)\cos\beta_t = T_{t1}$$

Equations of motion for gear *t*2:

$$m_{t2}\ddot{y}_{t2} - c_t\dot{p}_t(t) - \bar{k}_t p_t(t)\cos\beta_t\cos\psi_t = 0 \qquad \text{(2.11a-f)}$$

$$m_{t2}\ddot{x}_{t2} - c_t\dot{p}_t(t) - \bar{k}_t p_t(t)\cos\beta_t\sin\psi_t = 0$$

$$m_{t2}\ddot{z}_{t2} + c_t\dot{p}_t(t) + \bar{k}_t p_t(t)\sin\beta_t = 0$$

$$I_{t2}\ddot{\theta}_{yt2} + r_{t2}c_t\dot{p}_t(t) + r_{t2}\bar{k}_t p_t(t)\sin\beta_t\cos\psi_t = 0$$

$$I_{t2}\ddot{\theta}_{xt2} + r_{t2}c_t\dot{p}_t(t) + r_{t2}\bar{k}_t p_t(t)\sin\beta_t\sin\psi_t = 0$$

$$J_{t2}\ddot{\theta}_{zt2} + r_{t2}c_t\dot{p}_t(t) + r_{t2}\bar{k}_t p_t(t)\cos\beta_t = -T_{t2}$$

In these equations, $p_t(t)$ represents the relative displacement at the test gear mesh in the direction normal to contact surfaces defined by

$$\begin{aligned} p_t(t) = &\left[(x_{t1} - x_{t2})\sin\psi_t + (y_{t1} - y_{t2})\cos\psi_t + r_{t1}\theta_{zt1} + r_{t2}\theta_{zt2}\right]\cos\beta_t \\ &+ \left[-z_{t1} + z_{t2} + (r_{t1}\theta_{xt1} + r_{t2}\theta_{xt2})\sin\psi_t + (r_{t1}\theta_{yt1} + r_{t2}\theta_{yt2})\cos\psi_t\right]\sin\beta_t - e_t(t) \end{aligned} \tag{2.12}$$

The stiffness coupling matrix and the mass matrix of the gear pair *t* are obtained from equations (2.10-2.12) as

$$\mathbf{k}_t = \begin{bmatrix} (\mathbf{k}_{11})_t & (\mathbf{k}_{12})_t \\ (\mathbf{k}_{21})_t & (\mathbf{k}_{22})_t \end{bmatrix}, \tag{2.13}$$

$$\mathbf{M}_t = \begin{bmatrix} \mathbf{m}_{t1} & \mathbf{0} \\ \mathbf{0} & \mathbf{m}_{t2} \end{bmatrix}. \tag{2.14}$$

The corresponding displacement and alternating force vectors are given as

$$\mathbf{q}_t = \begin{Bmatrix} \mathbf{q}_{t1} \\ \mathbf{q}_{t2} \end{Bmatrix}, \tag{2.15}$$

$$\mathbf{F}_t(t) = \begin{Bmatrix} (\mathbf{f}_1)_t \\ (\mathbf{f}_2)_t \end{Bmatrix} e_t(t) \tag{2.16}$$

where $\mathbf{q}_{ti} = \begin{bmatrix} y_{ti} & x_{ti} & z_{ti} & \theta_{yti} & \theta_{xti} & \theta_{zti} \end{bmatrix}^T$ and $i = 1, 2$.

The above formulation can be repeated for the reaction gear pair formed by gears $r1$ (on the shaft 1) and $r2$ (on the shaft 2) to obtain the stiffness and mass matrices of the reaction gear pair as well by simply replacing the subscript t by subscript r in above equations with

$$\psi_r = \begin{cases} -\phi_r, & T_{t1} : counter\ clockwise \\ \phi_r, & T_{t1} : clockwise \end{cases} \tag{2.17}$$

$$\beta_r = \begin{cases} (+)ve & if\ \ gear\ \ r1\ has\ \ left\ \ hand\ \ teeth \\ (-)ve & if\ \ gear\ \ r1\ has\ \ right\ \ hand\ \ teeth \end{cases} \tag{2.18}$$

Accordingly, mass and stiffness matrices and the force and displacement vectors for the reaction gear pair are found to be:

$$\mathbf{k}_r = \begin{bmatrix} (\mathbf{k}_{11})_r & (\mathbf{k}_{12})_r \\ (\mathbf{k}_{21})_r & (\mathbf{k}_{22})_r \end{bmatrix}, \qquad \mathbf{M}_r = \begin{bmatrix} \mathbf{m}_{r1} & \mathbf{0} \\ \mathbf{0} & \mathbf{m}_{r2} \end{bmatrix}, \tag{2.19a,b}$$

$$\mathbf{q}_r = \begin{Bmatrix} \mathbf{q}_{r1} \\ \mathbf{q}_{r2} \end{Bmatrix}, \qquad \mathbf{F}_r(t) = \begin{Bmatrix} (\mathbf{f}_1)_r \\ (\mathbf{f}_2)_r \end{Bmatrix} e_r(t) \tag{2.20a,b}$$

The system shown in Figure 1.1(b) has a total of two shafts and four gears forming two gear pairs connecting certain degrees of freedom of each shaft to each other according to the formulation given above. The overall gear stiffness matrix and the mass matrix, both of dimension *S*, can be assembled in the form

$$\mathbf{K}_g = \begin{bmatrix} \ddots & & & & & & & \\ & (\mathbf{k}_{11})_t & & & & \textit{symm.} & & \\ & \vdots & \ddots & & & & & \\ & \mathbf{0} & \cdots & (\mathbf{k}_{11})_r & & & & \\ & \vdots & & \vdots & \ddots & & & \\ & (\mathbf{k}_{21})_t & \cdots & \mathbf{0} & \cdots & (\mathbf{k}_{22})_t & & \\ & \vdots & & \vdots & & \vdots & \ddots & \\ & \mathbf{0} & \cdots & (\mathbf{k}_{21})r & \cdots & \mathbf{0} & \cdots & (\mathbf{k}_{22})_r \\ & & & & & & & \ddots \end{bmatrix} \tag{2.21}$$

$$\mathbf{M}_g = Diag\begin{bmatrix} \cdots & \mathbf{m}_{t1} & \cdots & \mathbf{m}_{r1} & \cdots & \mathbf{m}_{t2} & \cdots & \mathbf{m}_{r2} & \cdots \end{bmatrix} \tag{2.22}$$

The masses and inertias of other non-gear components attached to a shaft must also be included in equation (2.22) at the appropriate nodes the same way the gear masses and inertias included.

2.1.4 Support Stiffness Matrices

In a typical application, each shaft is supported by least two rolling element bearings of varying type, size and design parameters. The most general way of describing

flexibility of an individual bearing is to define a 6x6 stiffness matrix $\mathbf{k}_{bi}$ with zero torsional terms [33, 36]. If there are n_b number of bearings in the system, an overall bearing stiffness matrix of dimension S can be constructed by assembling the individual stiffness matrices according to the shaft node at which each bearing is mounted

$$\mathbf{K}_b = \begin{bmatrix} \ddots & & & & & \\ \mathbf{0} & \mathbf{k}_{b1} & & & \textit{symm.} & \\ \vdots & \vdots & \ddots & & & \\ \mathbf{0} & \mathbf{0} & \cdots & \mathbf{k}_{b2} & & \\ \vdots & \vdots & \cdots & \vdots & \ddots & \\ \mathbf{0} & \mathbf{0} & \cdots & \mathbf{0} & \cdots & \mathbf{k}_{bn_b} \end{bmatrix}. \tag{2.23}$$

2.1.5 Equations of Motion

Given the mass and stiffness matrices for shafts, bearings/case and gears, the overall mass and stiffness matrices of the overall system are given as

$$\mathbf{M} = \mathbf{M}_s + \mathbf{M}_g \tag{2.24}$$

$$\mathbf{K} = \mathbf{K}_s + \mathbf{K}_b + \mathbf{K}_g \tag{2.25}$$

Finally, the force vector is defined in terms of the two static transmission error excitations as

$$\mathbf{F}(t)=\begin{Bmatrix}\vdots\\(\mathbf{f}_1)_t\,e_t(t)\\\vdots\\(\mathbf{f}_1)_r\,e_r(t)\\\vdots\\(\mathbf{f}_2)_t\,e_t(t)\\\vdots\\(\mathbf{f}_2)_r\,e_r(t)\\\vdots\end{Bmatrix}. \tag{2. 26}$$

The excitation function $e_t(t)$ at the mesh of the test gear pair includes only the once/mesh components of the static transmission error as index errors of actual gear specimens were considered to be insignificant

$$e_t(t)=\sum_{i=1}^{L}\tilde{e}_{ti}\sin\left[i\omega_t t+\varphi_{ti}\right] \tag{2.27}$$

where $\tilde{e}_{ti}$ is the *i*-th harmonic amplitude of the test gear pair transmission error .Here, the test gear mesh frequency is defined as $\omega_t=2\pi\Omega_{s1}Z_{t1}/60$ where Ω_{s1} is the rotational speed of the first shaft in *rpm* and Z_{t1} is the number of teeth on the first test gear. As evident form equation (2.27), no once/revolution component of the test gear mesh excitation is included since the pitch line run-out errors, index errors and spacing errors of the actual test gears were assumed to be negligible.

Similarly the excitation function $e_r(t)$ at the mesh of the reaction gear pair includes the once/mesh components of the static transmission error. Accordingly $e_r(t)$ is defined as

$$e_r(t) = \sum_{i=1}^{L} \tilde{e}_{ri} \sin\left[i\omega_r t + \varphi_{ri}\right] \tag{2.28}$$

Here $\tilde{e}_{ri}$ is the *i*-th harmonic mesh order amplitude of the reaction gear pair, and the reaction gear mesh frequency is defined as $\omega_r = 2\pi\Omega_{s1}Z_{r1}/60$ where Z_{r1} is the number of teeth on the first reaction gear.

2.1.6 Natural Modes and Forced Response

Equations of motion of the overall system can be written in matrix form as

$$\mathbf{M}\,\ddot{\mathbf{X}}(t) + \mathbf{C}\,\dot{\mathbf{X}}(t) + \mathbf{K}\,\mathbf{X}(t) = \mathbf{F}(t) \tag{2.29}$$

The transverse-torsional model formulation presented up to this point did not include the derivation of the damping matrix **C**. If the damping values of each component including gear meshes, bearings and shafts were known, one could obtain a damping matrix that is in the same form as **K**. However, these damping values are not known in most cases. Therefore, here for practical engineering purposes, a set of modal damping values ζ_i are

used to define **C** instead of using a damping matrix that is formed by actual damping values.

The eigen value problem governing equation (2.29) yield the natural frequencies ω_i and the corresponding modal vectors $\mathbf{\Phi}_i$ (mode shapes) where $i = 1, 2, \ldots, S$ is the modal index. The Sequential Jacobi Method is used here for the Eigen Value solutions as in the case of the a purely torsional six degree of freedom limiting case. The forced response of the system is obtained by using the same approach (Modal Summation Technique) [37] as the torsional model, now with the forcing vector given by equation (2.26) where $e_t(t)$ and $e_r(t)$ are defined by equations (2.27) and (2.28), respectively.

2.2 The Limiting Case: A Purely Torsional Model

A purely torsional linear dynamic model of a four-square gear durability test machine with flywheels shown in Figure 1.1(b) is developed here as shown in Figure 2.3. Here, each gear of base radius *r* and polar mass moment of inertia J is assumed to be rigid except the teeth in contact. Gears and flywheels are also assumed to vibrate in torsional direction only defined by rotational alternating displacement θ. The gear mesh interface of the test gears is represented by linear gear mesh stiffness $\bar{k}_t$ and a periodic static transmission error excitation $e_t(t)$. Similarly, $\bar{k}_r$ and $e_r(t)$ represent the mean mesh stiffness and the transmission error excitation of the reaction gear pair.

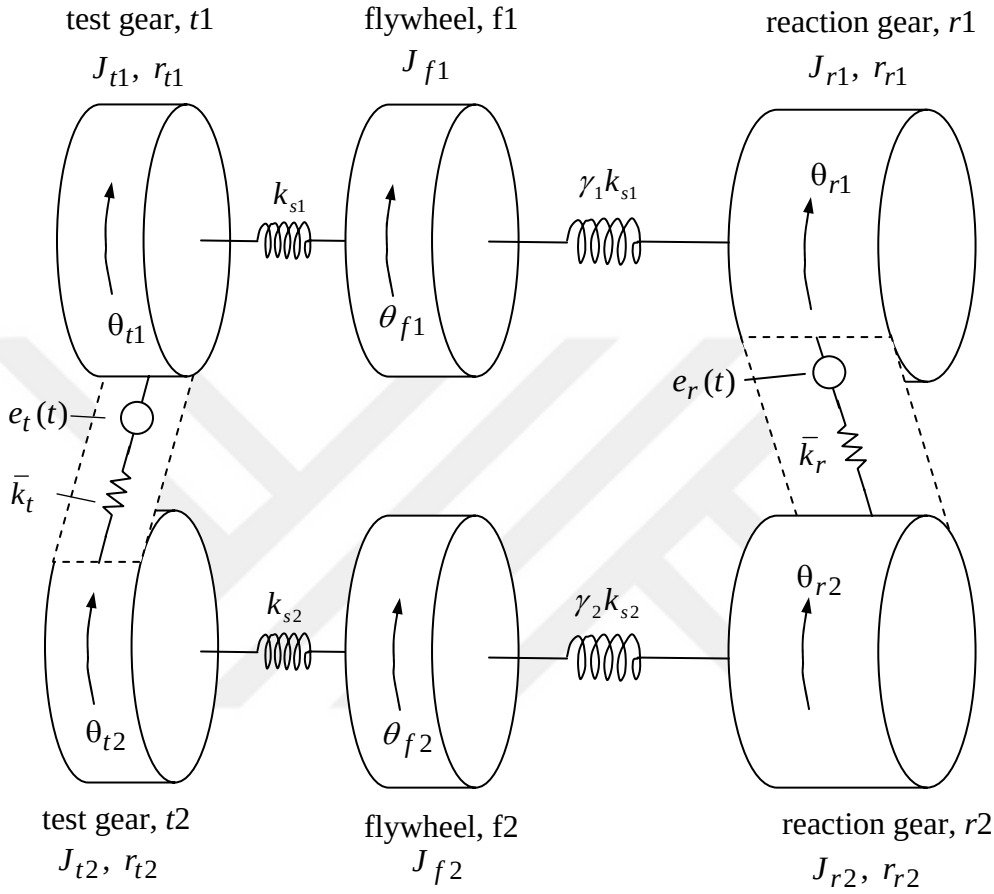

Figure 2.3. A six-degree-of-freedom torsional model of a four-square test machine.

2.2.1 Equations of Motion

Considering that the subscripts *t*1 and t2 represent test gears on shafts 1 and 2 and subscripts *r*1 and *r*2 represent the reaction gears on shafts 1 and 2, the equations of motion of the four-degree-of-freedom dynamic model are given as

$$\left.\begin{aligned}
&J_{t1}\ddot{\theta}_{t1} + r_{t1}c_t\left[r_{t1}\dot{\theta}_{t1} + r_{t2}\dot{\theta}_{t2}\right] + r_{t1}\bar{k}_t\left[r_{t1}\theta_{t1} + r_{t2}\theta_{t2} - e_t(t)\right] + k_{s1}(\theta_{t1} - \theta_{f1}) = 0\\
&J_{t2}\ddot{\theta}_{t2} + r_{t2}c_t\left[r_{t1}\dot{\theta}_{t1} + r_{t2}\dot{\theta}_{t2}\right] + r_{t2}\bar{k}_t\left[r_{t1}\theta_{t1} + r_{t2}\theta_{t2} - e_t(t)\right] + k_{s2}(\theta_{t2} - \theta_{f2}) = 0\\
&J_{f2}\ddot{\theta}_{f2} - k_{s2}(\theta_{t2} - \theta_{f2}) + \gamma_2 k_{s2}(\theta_{f2} - \theta_{r2}) = 0\\
&J_{r2}\ddot{\theta}_{r2} + r_{r2}c_r\left[r_{r1}\dot{\theta}_{r1} + r_{r2}\dot{\theta}_{r2}\right] + r_{r2}\bar{k}_r\left[r_{r1}\theta_{r1} + r_{r2}\theta_{r2} - e_r(t)\right] - \gamma_2 k_{s2}(\theta_{f2} - \theta_{r2}) = 0\\
&J_{r1}\ddot{\theta}_{r1} + r_{r1}c_r\left[r_{r1}\dot{\theta}_{r1} + r_{r2}\dot{\theta}_{r2}\right] + r_{r1}\bar{k}_r\left[r_{r1}\theta_{r1} + r_{r2}\theta_{r2} - e_r(t)\right] + \gamma_1 k_{s1}(\theta_{r1} - \theta_{f1}) = 0\\
&J_{f1}\ddot{\theta}_{f1} - \gamma_1 k_{s1}(\theta_{r1} - \theta_{f1}) - k_{s1}(\theta_{t1} - \theta_{f1}) = 0
\end{aligned}\right\} \quad (2.30)$$

where c_t and c_r represent the gear mesh damping values that are not shown in Figure 2.3 for clarity purposes, and k_{s1} and k_{s2} are the torsional stiffness values of the shafts connecting the test gears to the flywheels and $\gamma_1 k_{s1}$,and $\gamma_2 k_{s2}$ are the torsional stiffness values of the shafts connecting the test gears to the reaction gears. The polar mass moments of inertia of these shafts are divided into two and lumped to the inertias of the gears at both sides. In order to obtain a matrix form of the equations of motion, equation (2.30) can be put into the form:

$$\left.\begin{aligned}
&J_{t1}\ddot{\theta}_{t1}+r_{t1}^2c_t\dot{\theta}_{t1}+r_{t1}r_{t2}c_t\dot{\theta}_{t2}+(r_{t1}^2\bar{k}_t+k_{s1})\theta_{t1}+r_{t1}r_{t2}\bar{k}_t\theta_{t2}-k_{s1}\theta_{f1}=r_{t1}\bar{k}_te_t(t)\\
&J_{t2}\ddot{\theta}_{t2}+r_{t1}r_{t2}c_t\dot{\theta}_{t1}+r_{t2}^2c_t\dot{\theta}_{t2}+r_{t1}r_{t2}\bar{k}_t\theta_{t1}+(r_{t2}^2\bar{k}_t+k_{s2})\theta_{t2}-k_{s2}\theta_{f2}=r_{t2}\bar{k}_te_t(t)\\
&J_{f2}\ddot{\theta}_{f2}-k_{s2}\theta_{t2}+(k_{s2}+\gamma_2k_{s2})\theta_{f2}-\gamma_2k_{s2}\theta_{r2}=0\\
&J_{r2}\ddot{\theta}_{r2}-\gamma_2k_{s2}\theta_{f2}+r_{r2}^2c_r\dot{\theta}_{r2}+r_{r1}r_{r2}c_r\dot{\theta}_{r1}+r_{r1}r_{r2}\bar{k}_r\theta_{r1}+(r_{r2}^2\bar{k}_r+k_{s2})\theta_{r2}=r_{r2}\bar{k}_re_r(t)\\
&J_{r1}\ddot{\theta}_{r1}-\gamma_1k_{s1}\theta_{f1}+r_{r1}r_{r2}c_r\dot{\theta}_{r2}+r_{r1}^2c_r\dot{\theta}_{r1}+r_{r1}r_{r2}\bar{k}_r\theta_{r2}+(r_{r1}^2\bar{k}_r+k_{s1})\theta_{r1}=r_{r1}\bar{k}_re_r(t)\\
&J_{f1}\ddot{\theta}_{f1}-k_{s1}\theta_{t1}+(k_{s1}+\gamma_1k_{s1})\theta_{f1}-\gamma_1k_{s1}\theta_{r1}=0
\end{aligned}\right\} \quad (2.31)$$

The equations of motion are then written in matrix form as

$$\mathbf{M}\ddot{\mathbf{q}}(t)+\mathbf{C}\dot{\mathbf{q}}(t)+\mathbf{K}\mathbf{q}(t)=\mathbf{F}(t) \quad (2.32a)$$

where the mass, damping and stiffness matrices are defined as

$$\mathbf{M}=\begin{bmatrix} J_{t1} & 0 & 0 & 0 & 0 & 0\\ 0 & J_{t2} & 0 & 0 & 0 & 0\\ 0 & 0 & J_{f2} & 0 & 0 & 0\\ 0 & 0 & 0 & J_{r2} & 0 & 0\\ 0 & 0 & 0 & 0 & J_{r1} & 0\\ 0 & 0 & 0 & 0 & 0 & J_{f1} \end{bmatrix}, \quad (2.32b)$$

$$\mathbf{C} = \begin{bmatrix} r_{t1}^2 c_t & r_{t1} r_{t2} c_t & 0 & 0 & 0 & 0 \\ r_{t1} r_{t2} c_t & r_{t2}^2 c_t & 0 & 0 & 0 & 0 \\ 0 & 0 & 0 & 0 & 0 & 0 \\ 0 & 0 & 0 & r_{r2}^2 c_r & r_{r1} r_{r2} c_r & 0 \\ 0 & 0 & 0 & r_{r1} r_{r2} c_r & r_{r1}^2 c_t & 0 \\ 0 & 0 & 0 & 0 & 0 & 0 \end{bmatrix} \tag{2.32c}$$

$$\mathbf{K} = \begin{bmatrix} r_{t1}^2 \bar{k}_t + k_{s1} & r_{t1} r_{t2} \bar{k}_t & 0 & 0 & 0 & -k_{s1} \\ r_{t1} r_{t2} \bar{k}_t & r_{t2}^2 \bar{k}_t + k_{s2} & -k_{s2} & 0 & 0 & 0 \\ 0 & -k_{s2} & k_{s2} + \gamma_2 k_{s2} & -\gamma_2 k_{s2} & 0 & 0 \\ 0 & 0 & -\gamma_2 k_{s2} & r_{r2}^2 \bar{k}_r + \gamma_2 k_{s2} & r_{r1} r_{r2} \bar{k}_r & 0 \\ 0 & 0 & 0 & r_{r1} r_{r2} \bar{k}_r & r_{r1}^2 \bar{k}_r + \gamma_1 k_{s1} & -\gamma_1 k_{s1} \\ -k_{s1} & 0 & 0 & 0 & -\gamma_{s1} k_{s1} & k_{s1} + \gamma_1 k_{s1} \end{bmatrix} \tag{2.32d}$$

The displacement vector and the external forcing vector are defined as

$$\mathbf{q}(t) = \begin{Bmatrix} \theta_{t1}(t) \\ \theta_{t2}(t) \\ \theta_{f2}(t) \\ \theta_{r2}(t) \\ \theta_{r1}(t) \\ \theta_{f1}(t) \end{Bmatrix}, \qquad \mathbf{F}(t) = \begin{Bmatrix} r_{t1} \bar{k}_t e_t(t) \\ r_{t1} \bar{k}_t e_t(t) \\ 0 \\ r_{r2} \bar{k}_r e_r(t) \\ r_{r1} \bar{k}_r e_r(t) \\ 0 \end{Bmatrix}. \tag{2.32e,f}$$

The excitation function $e_t(t)$ is taken to be same as that of the three dimensional dynamic model as given in equation (2.27).

Unlikely the equation (2.28), the excitation function $e_r(t)$ at the mesh of the reaction gear pair includes not only the once/mesh components of the static transmission

error but also once/revolution components of each reaction gear since indexing errors of these gears are assumed to be not negligible. Accordingly $e_r(t)$ is defined as

$$e_r(t) = \sum_{i=1}^{L} \tilde{e}_{ri} \sin\left[i\omega_r t + \varphi_{ri}\right] + E_{r1} \sin\left[\frac{\omega_r}{Z_{r1}} t + \delta_{r1}\right] - E_{r2} \sin\left[\frac{\omega_r}{Z_{r2}} t + \delta_{r2}\right]. \tag{2.33}$$

In addition to equation (2.28), the once/revolution errors of both reaction gears are included in harmonic form having amplitudes E_{r1} and E_{r2} and initial assembly position angles δ_{r1} and δ_{r2}. The frequency of these two excitations are ω_r / Z_{r1} and ω_r / Z_{r2}.

2.2.2 Natural Modes and Forced Response

The solution of the Eigen Value problem governing equation (2.32a) yields the natural frequencies ω_i and the corresponding modal vectors (mode shapes) $\mathbf{\Phi}_i$ ($i = 1$ to 6). The system shown in Figure 2.3 does not have any non-linearities, the forced response to the excitations of equations (2.27) and (2.33) can be calculated by using the Modal Summation Technique [37]. In order to apply this technique, first the forcing vector $\mathbf{F}(t)$ of equation (2.32f) is put in the form

$$\mathbf{F}(t)=\begin{Bmatrix} r_{t1}\\ r_{t2}\\ 0\\ 0\\ 0\\ 0 \end{Bmatrix}\bar{k}_t\sum_{i=1}^{L}\tilde{e}_{ti}\sin\left[i\omega_t t+\varphi_{ti}\right]+\begin{Bmatrix} 0\\ 0\\ 0\\ r_{r2}\\ r_{r1}\\ 0 \end{Bmatrix}\bar{k}_r\sum_{i=1}^{L}\tilde{e}_{ri}\sin\left[i\omega_r t+\varphi_{ri}\right]$$
$$+\begin{Bmatrix} 0\\ 0\\ 0\\ r_{r2}\\ r_{r1}\\ 0 \end{Bmatrix}\bar{k}_r E_{r1}\sin\left[\frac{\omega_r}{Z_{r1}}t+\delta_{r1}\right]-\begin{Bmatrix} 0\\ 0\\ 0\\ r_{r2}\\ r_{r1}\\ 0 \end{Bmatrix}\bar{k}_r E_{r2}\sin\left[\frac{\omega_r}{Z_{r2}}t+\delta_{r2}\right] \tag{2.34}$$

The forced response $\mathbf{q}(t)$ is then defined as

$$\mathbf{q}(\mathrm{t})=\begin{Bmatrix} r_{t1}\\ r_{t2}\\ 0\\ 0\\ 0\\ 0 \end{Bmatrix}\bar{k}_t\sum_{i=1}^{L}\mathbf{\Lambda}_{ti}\tilde{e}_{ti}\sin\left[i\omega_t t+\varphi_{ti}+\Gamma_{ti}\right]+\begin{Bmatrix} 0\\ 0\\ 0\\ r_{r2}\\ r_{r1}\\ 0 \end{Bmatrix}\bar{k}_r\sum_{i=1}^{L}\mathbf{\Lambda}_{ri}\tilde{e}_{ri}\sin\left[i\omega_r t+\varphi_{ri}+\Gamma_{ri}\right]$$
$$+\begin{Bmatrix} 0\\ 0\\ 0\\ r_{r2}\\ r_{r1}\\ 0 \end{Bmatrix}\bar{k}_r\mathbf{\Lambda}_{E1}E_{r1}\sin\left[\frac{\omega_r}{Z_{r1}}t+\delta_{r1}+\Gamma_{E1}\right]-\begin{Bmatrix} 0\\ 0\\ 0\\ r_{r2}\\ r_{r1}\\ 0 \end{Bmatrix}\bar{k}_r\mathbf{\Lambda}_{E2}E_{r2}\sin\left[\frac{\omega_r}{Z_{r2}}t+\delta_{r2}+\Gamma_{E2}\right] \tag{2.35a}$$

where the dynamic compliance matrices are

$$\mathbf{\Lambda}_{ti} = \sum_{s=1}^{S} \frac{\mathbf{\Phi}_s \mathbf{\Phi}_s{}^T}{(\omega_s{}^2 - i^2 \omega_t{}^2 + 2jr\zeta_s \omega_s \omega_t)}, \tag{2.35b}$$

$$\mathbf{\Lambda}_{ri} = \sum_{s=1}^{S} \frac{\mathbf{\Phi}_s \mathbf{\Phi}_s{}^T}{(\omega_s{}^2 - i^2 \omega_r{}^2 + 2jr\zeta_s \omega_s \omega_r)}, \tag{2.35c}$$

$$\mathbf{\Lambda}_{E1} = \sum_{s=1}^{S} \frac{\mathbf{\Phi}_s \mathbf{\Phi}_s{}^T}{(\omega_s{}^2 - \left(\frac{\omega_r}{Z_{r1}}\right)^2 + \frac{2jr\zeta_s \omega_s \omega_r}{Z_{r1}})}, \tag{2.35d}$$

$$\mathbf{\Lambda}_{E2} = \sum_{s=1}^{S} \frac{\mathbf{\Phi}_s \mathbf{\Phi}_s{}^T}{(\omega_s{}^2 - \left(\frac{\omega_r}{Z_{r2}}\right)^2 + \frac{2jr\zeta_s \omega_s \omega_r}{Z_{r2}})}. \tag{2.35e}$$

In above equations, L is the number of static transmission error harmonics that must be included in the analysis. Typically, it is sufficient to set $\mathrm{L} = 3$ for spur gears as the higher harmonic amplitudes $(\mathrm{i} > 3)$ are negligibly small. S is the total number of degrees of freedom considered in the model. For the system in Figure 2.3, $\mathrm{S} = 6$.

CHAPTER 3

RESULTS AND DISCUSSIONS

3.1 FZG Gear Test Machine

The FZG gear test machine illustrated in Figure 1.3 is a four-square type gear test machine with mechanical power circulation. This machine was originally developed in Germany in early 70s and became one of the standard tests machines for evaluating gear pitting and scuffing.

Figure 3.1 shows the assembly drawing of an FZG test machine. Three-dimensional model of it is shown in Figure 3.2. Total number of degrees of freedom for the system in Figure 3.2, S=150. Here both 3D model and 6-DOF model are used to study this system. The dynamic forces at the gear mesh are of particular interest here since the durability of the test gear is heavily dependent on the loads carried by the gear mesh. The transmission error excitation harmonic amplitudes are taken as $\tilde{e}_{t1} = 1.0\ \mu m$ and $\tilde{e}_{r1} = 1.0\ \mu m$. A 5 percent of damping coefficient value is considered. Gear mesh stiffness values are estimated to be $\bar{k}_t = 6 \times 10^7\ N/m$ and $\bar{k}_r = 6 \times 10^7\ N/m$. Table 3.1 summarizes all the parameters required by the dynamic model. The dynamic gear mesh force amplitudes are given in Figure 3.3. The main resonance peaks appear at 2400 and 2700 rpm on reaction and test gear meshes, respectively. These resonances occur when

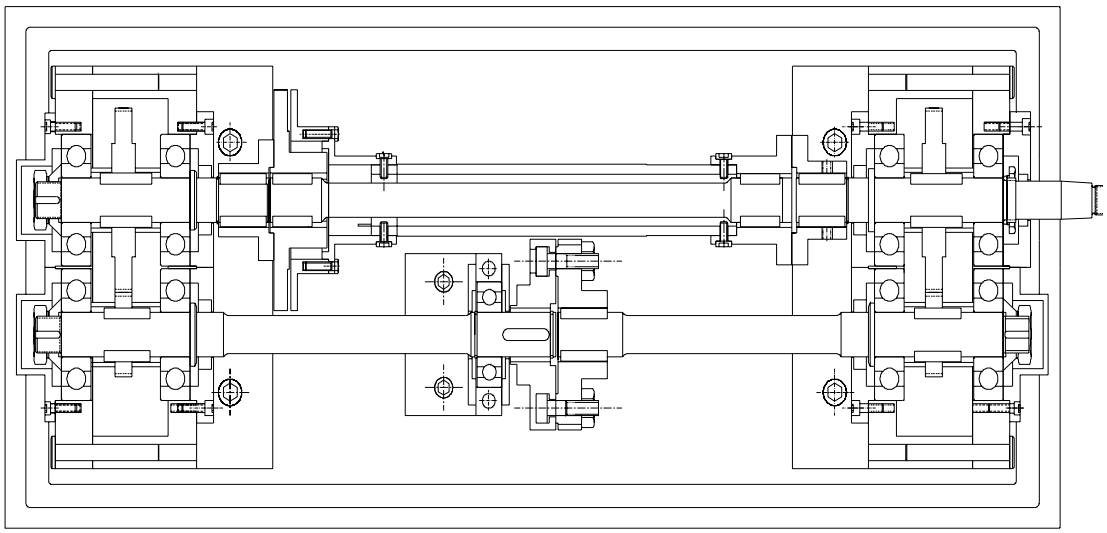

Figure 3.1 Technical drawing of FZG gear test machine.

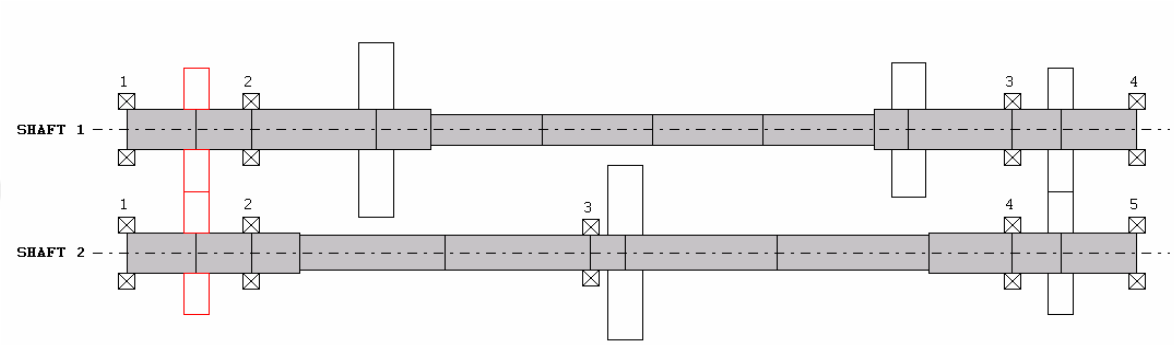

Figure 3.2 Dynamic model of FZG gear test machine

Table 3.1

System parameters of the FZG Gear Test Machine

Diameter of test gears	$0.092\ m$
Number of teeth of test gears	45
Diameter of reaction gears	$0.092\ m$
Number of teeth of reaction gears	50
Test gear mesh stiffness	$6.0\times10^{7}\ N/m$
Reaction gear mesh stiffness	$6.0\times10^{7}\ N/m$
Mass of test gears	$0.850\,kg$
Mass of reaction gears	$0.850\,kg$
Polar moment of inertia of test gears	$1.0\times10^{-3}\ kg-m^{2}$
Polar moment of inertia of reaction gears	$1.0\times10^{-3}\ kg-m^{2}$
Diameter of Shaft 1	0.030 and $0.023\ m$
Diameter of Shaft 2	0.030 and $0.026\ m$
Polar moment of inertia of first inertia element in Shaft 1	$11.5\times10^{-3}\ kg-m^{2}$
Mass of the first inertia element in Shaft 1	$5.5\,kg$
Polar moment of inertia of second inertia element in Shaft 1	$1.0\times10^{-3}\ kg-m^{2}$
Mass of second inertia element in Shaft 1	$2.5\,kg$
Polar moment of inertia of the inertia element in Shaft 2	$10.8\times10^{-3}\ kg-m^{2}$
Mass of inertia element in Shaft 2	$5.4\,kg$

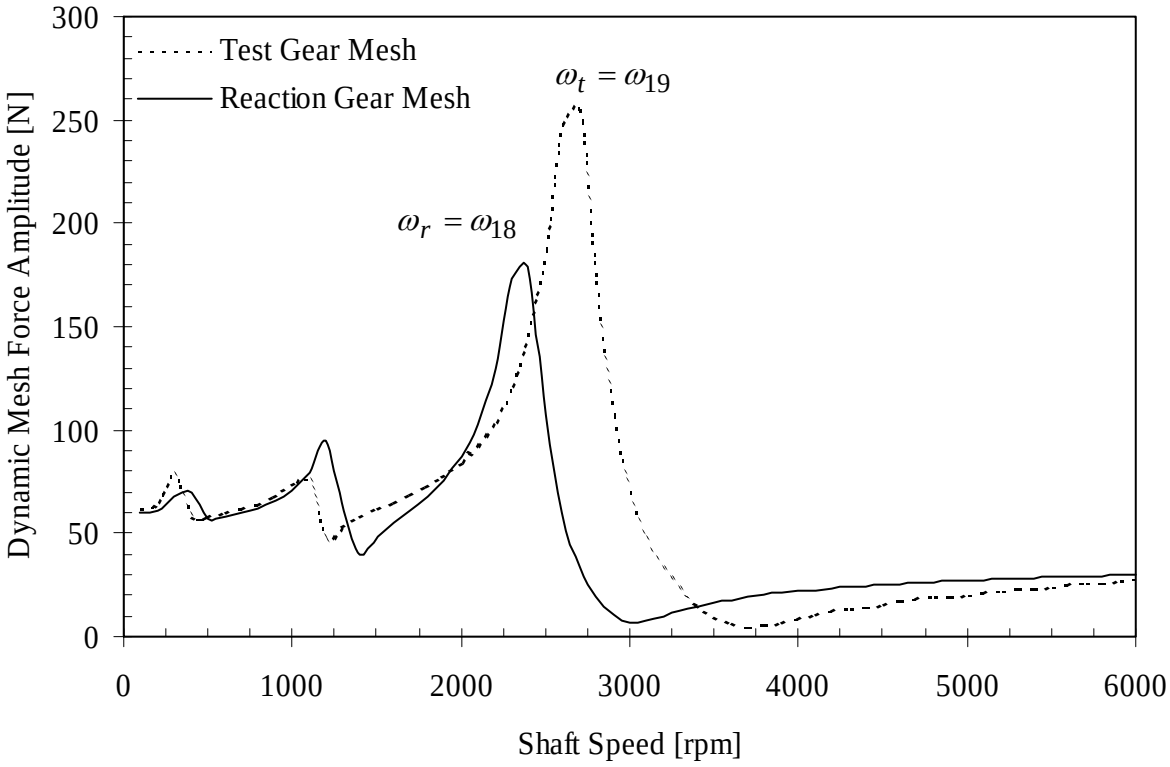

Figure 3.3 Dynamic mesh force amplitude of the test and reaction gear pair of FZG gear test machine due to $\tilde{e}_{r1} = 1.0\ \mu m$ and $\tilde{e}_{t1} = 1.0\ \mu m$.

the reaction and test gear mesh frequencies are equal to natural frequencies at 1986 and 2008 Hz, respectively.

In order to examine the force and vibration transmissibility of the system, first transmission error harmonic amplitudes are taken to be $\tilde{e}_{t1} = 0.0\ \mu m$ and $\tilde{e}_{r1} = 1.0\ \mu m$. Since there is no excitation applied on the test gear mesh, any dynamic loads on the test gear mesh must be due to the excitation applied to the reaction side. From Figure 3.4, test gear dynamic mesh force amplitudes are almost zero, suggesting that long and slender connecting shafts offer a good isolation of test side from reaction side. A similar analysis was done to investigate the effect of the test side on the reaction side. This time, transmission error harmonic amplitudes are taken to be $\tilde{e}_{t1} = 1.0\ \mu m$ and $\tilde{e}_{r1} = 0.0\ \mu m$. Similar to Figure 3.4, there is no tangible dynamic loads on reaction gear mesh due to the disturbances of the test side again indicating good isolation characteristics in Figure 3.5.

When the higher harmonics of the test and reaction gear mesh excitation are also included, the response curves become more complex while still two of the modes are excited within the speed range considered. Figure 3.6 shows the dynamic response for this case.

The modes excited at frequencies $\omega_r = \omega_{18}$ and $\omega_t = \omega_{19}$ are shown in Figure 3.7. In Figure 3.7(a), all gears and inertias rotate torsionally. In addition, the reaction gear on the first shaft also translates in both x and y direction. The relative gear mesh displacement at the reaction gear mesh displacement is large, causing this mode to be excited by transmission error excitation. In Figure 3.7(b), similar situation exists for the test gear. All of the natural modes with frequencies less than 5000 Hz are listed in Table 3.2.

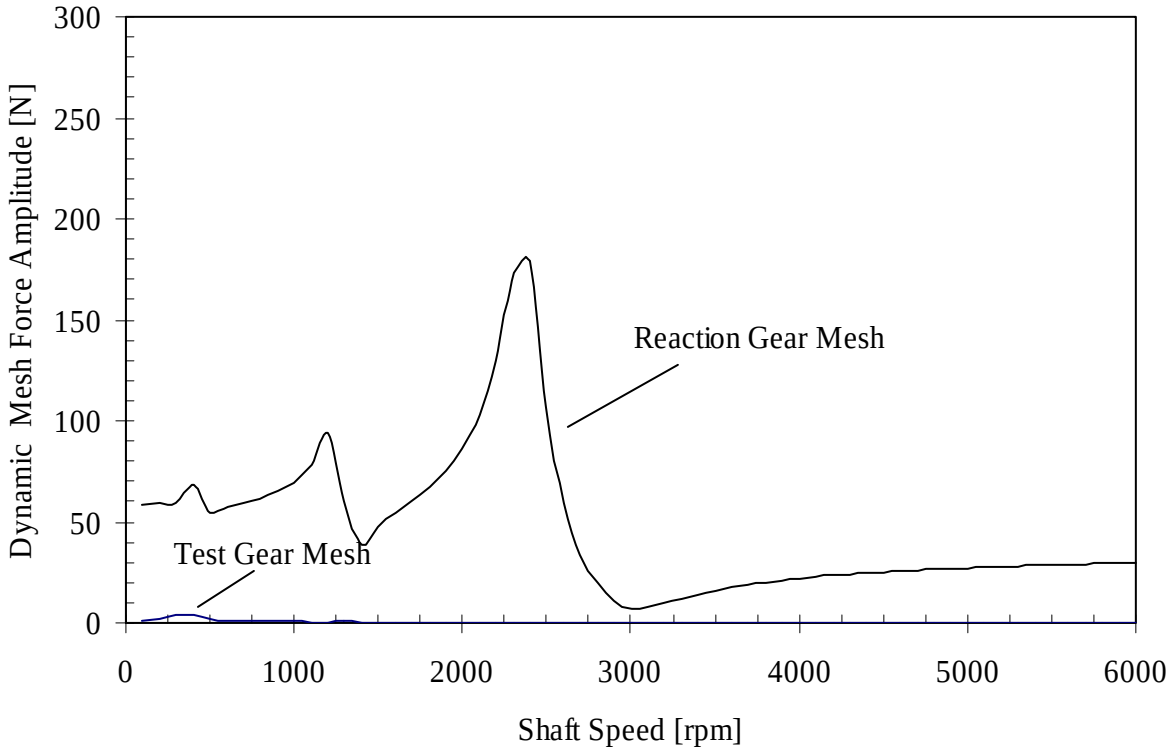

Figure 3.4 Dynamic mesh force amplitude of the test and reaction gear pair of FZG gear test machine due to $\tilde{e}_{r1} = 1.0\ \mu m$ and $\tilde{e}_{t1} = 0.0\ \mu m$.

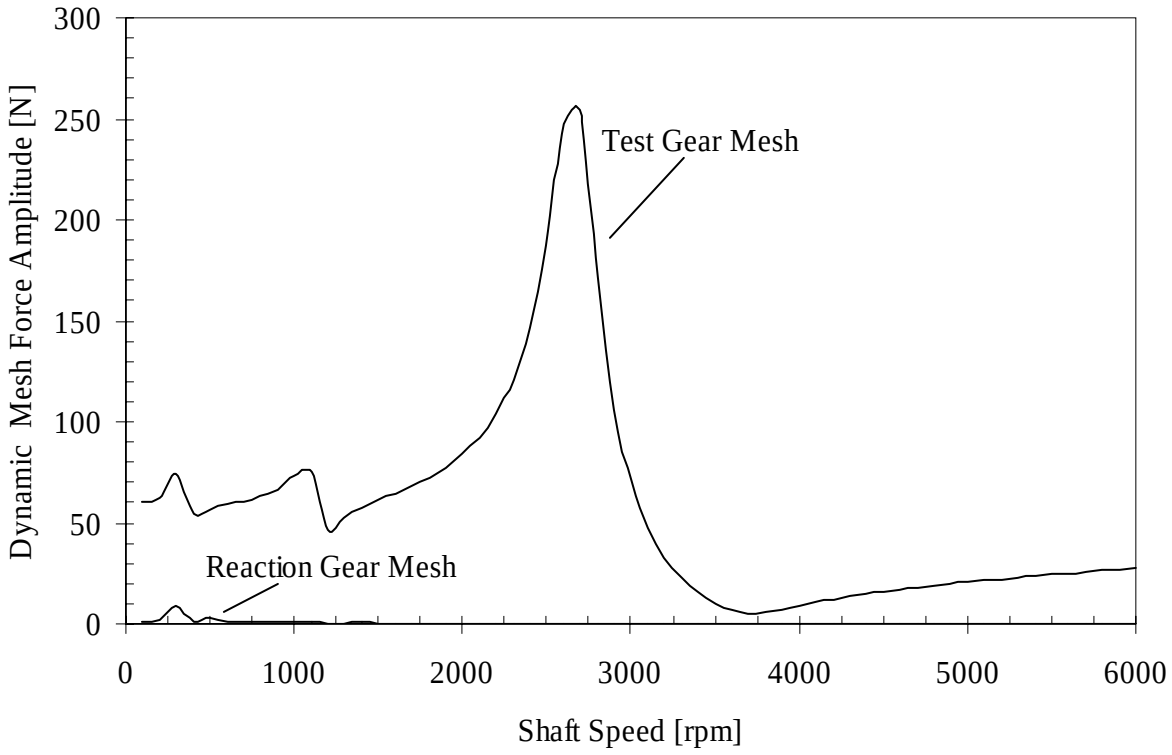

Figure 3.5 Dynamic mesh force amplitude of the test and reaction gear pair of FZG gear test machine due to $\tilde{e}_{r1} = 0.0\ \mu m$ and $\tilde{e}_{t1} = 1.0\ \mu m$.

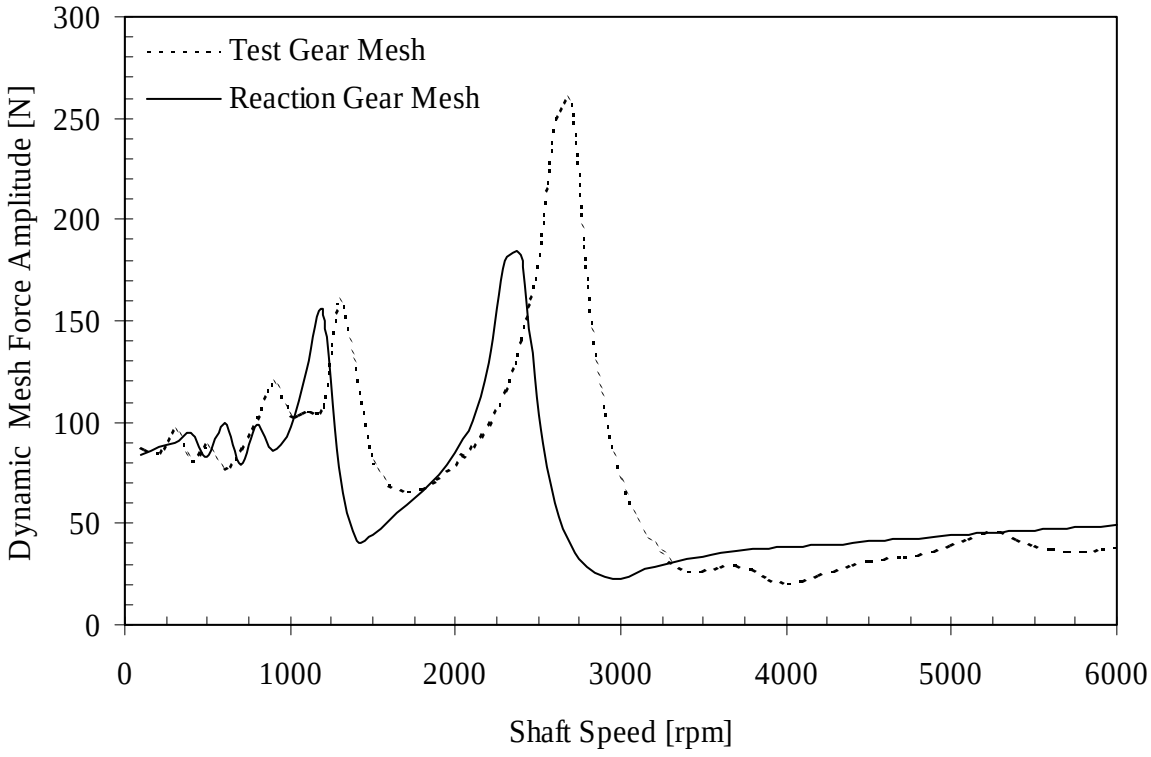

Figure 3.6 Dynamic mesh force amplitude of the test and reaction gear pair of FZG test machine due to $\tilde{e}_{r1} = 1.0\ \mu m$, $\tilde{e}_{r2} = 0.5\ \mu m$, $\tilde{e}_{r3} = 0.25\ \mu m$ and $\tilde{e}_{t1} = 1.0\ \mu m$, $\tilde{e}_{t2} = 0.5\ \mu m$, $\tilde{e}_{t3} = 0.25\ \mu m$.

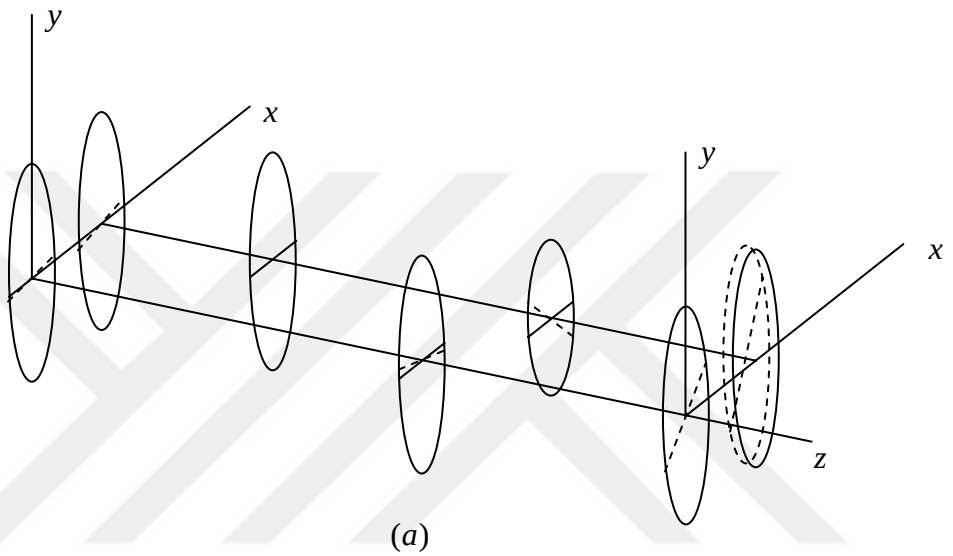

Figure 3.7 Mode shape of FZG gear test machine at (a) 1987 *Hz* and (b) 2008 *Hz*

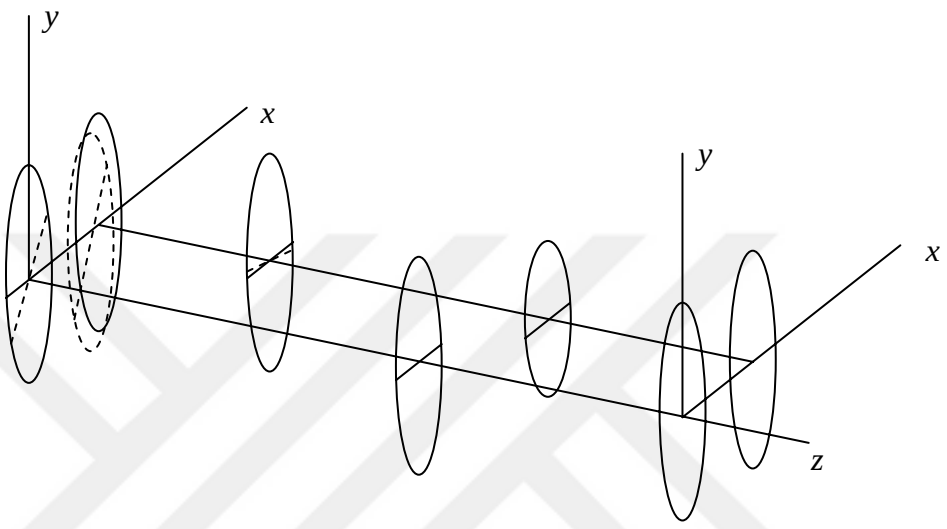

(*b*)

Figure 3.7 Continued.

Table 3.2

Natural modes of the FZG gear test machine. Double modes are marked (*).

Modes	Frequencies (Hz)	Description
1	0.0	Rigid body mode
2	232.2	Torsional
3, 4	332.3 (*)	Bending of Shaft 1 in x and y directions
5	345.8	Torsional
6, 7	605.9 (*)	Bending of Shaft 1 in x and y directions
8, 9	641.7 (*)	Bending of both shafts in x and y direction
10	833.3	Torsional
11	1056.0	Torsional
12, 13	1085.4 (*)	Bending of Shaft 1 in x and y directions and torsion of both shafts
14, 15	1517.2	Bending of Shaft 1 in x and y directions torsion of shafts
16, 17	1815.4 (*)	Bending of Shaft 2 in x and y directions
18	1986.7	Mode shape is shown in Figure 3.7
19	2008.9	Mode shape is shown in Figure 3.7
20, 21	2015.1 (*)	Bending of Shaft 2 in x and y directions
22, 23	2162.3 (*)	Bending of Shaft 2 in x and y directions and torsion of both shafts
24, 25	2396.5 (*)	Bending of Shaft 1 in x and y directions and torsion of both shafts
26	2659.1	Bending of Shaft 1 in y direction
27	3286.1	Bending of Shaft 2 in y direction
28, 29	3391.5 (*)	Bending of Shaft 1 in x and y directions
30	4150.5	Bending of Shaft 1 in x direction
31, 32	4747.0 (*)	Bending of Shaft 1 in x and y directions
33	4768.7	Torsional

Next, the same system analyzed by using 6-DOF model. Shafts inertias are lumped to the gears and flywheels. The same operating condition and excitation levels are maintained. Figure 3.8 compares the dynamic gear test mesh force amplitudes obtained by using 3D model and the torsional model for $\tilde{e}_{t1} = 1.0\ \mu m$ and $\tilde{e}_{r1} = 1.0\ \mu m$. The agreement between the 3D and torsional model is rather good especially for practical engineering purposes. Since the 3D model capable of representing the actual system more accurately, the differences between the results of two model can be attributed to the errors associated with torsional model.

3.2 Gear Dynamic Test Machine

As the second example, a gear dynamic test machine available at the Center for Gear Research is used. This machine shown in Figures 1.4 and 3.9 is also a four-square arrangement. The machine consists of a test gear pair, a reaction gear pair, and flexible shafts with two large flywheels in between.

With the large flywheels in between, this system lends itself to be an application of the 6-DOF dynamic model developed earlier. System parameters are given in Table 3.3. The main characteristic investigated here again is force and vibration transmissibility. Excitations are due to the transmission error harmonic amplitudes which are taken to be $\tilde{e}_{t1} = 1.0\,\mu m$ and $\tilde{e}_{r1} = 1.0\ \mu m$. A 5 percent of damping coefficient value is taken like the previous example. Gear mesh stiffness values are estimated to be $\bar{k}_t = 2.5 \times 10^8\ N/m$ and $\bar{k}_r = 5 \times 10^8\ N/m$ the dynamic mesh force amplitudes found by the torsional model

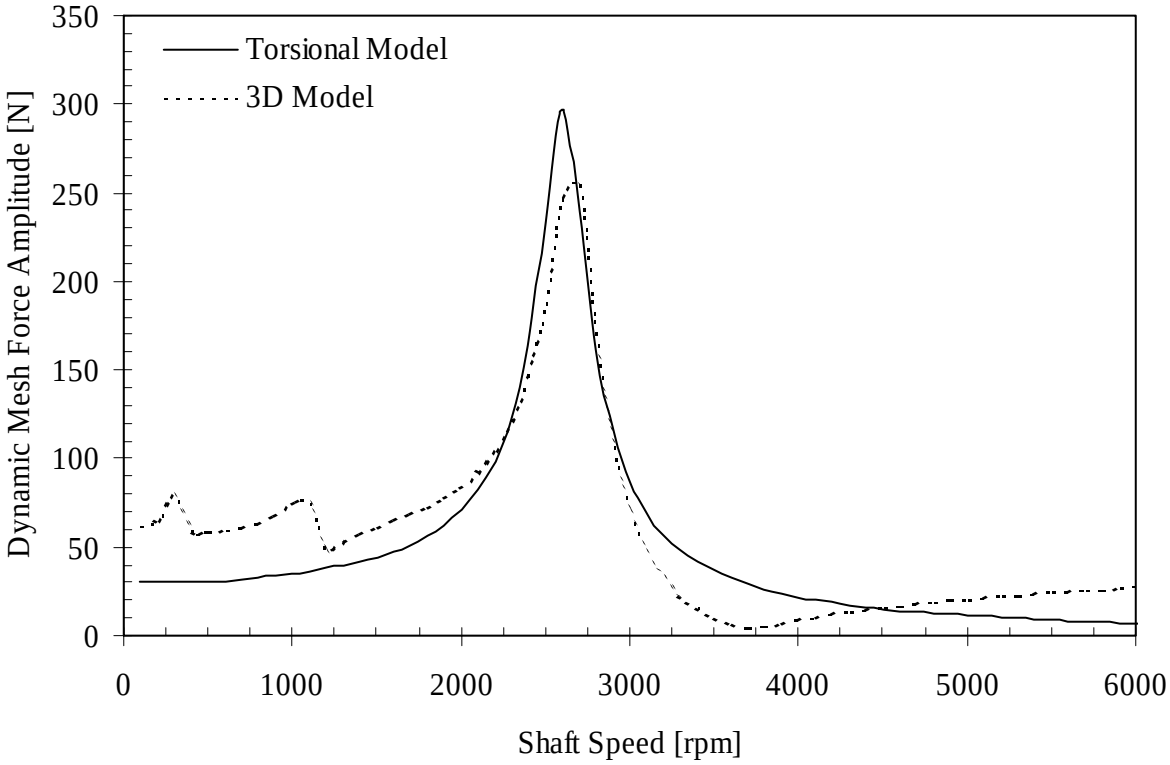

Figure 3.8 Comparison of dynamic mesh force amplitude of the test gear pair of the FZG test machine for $\tilde{e}_{t1} = 1.0\ \mu m$ and $\tilde{e}_{r1} = 1.0\ \mu m$.

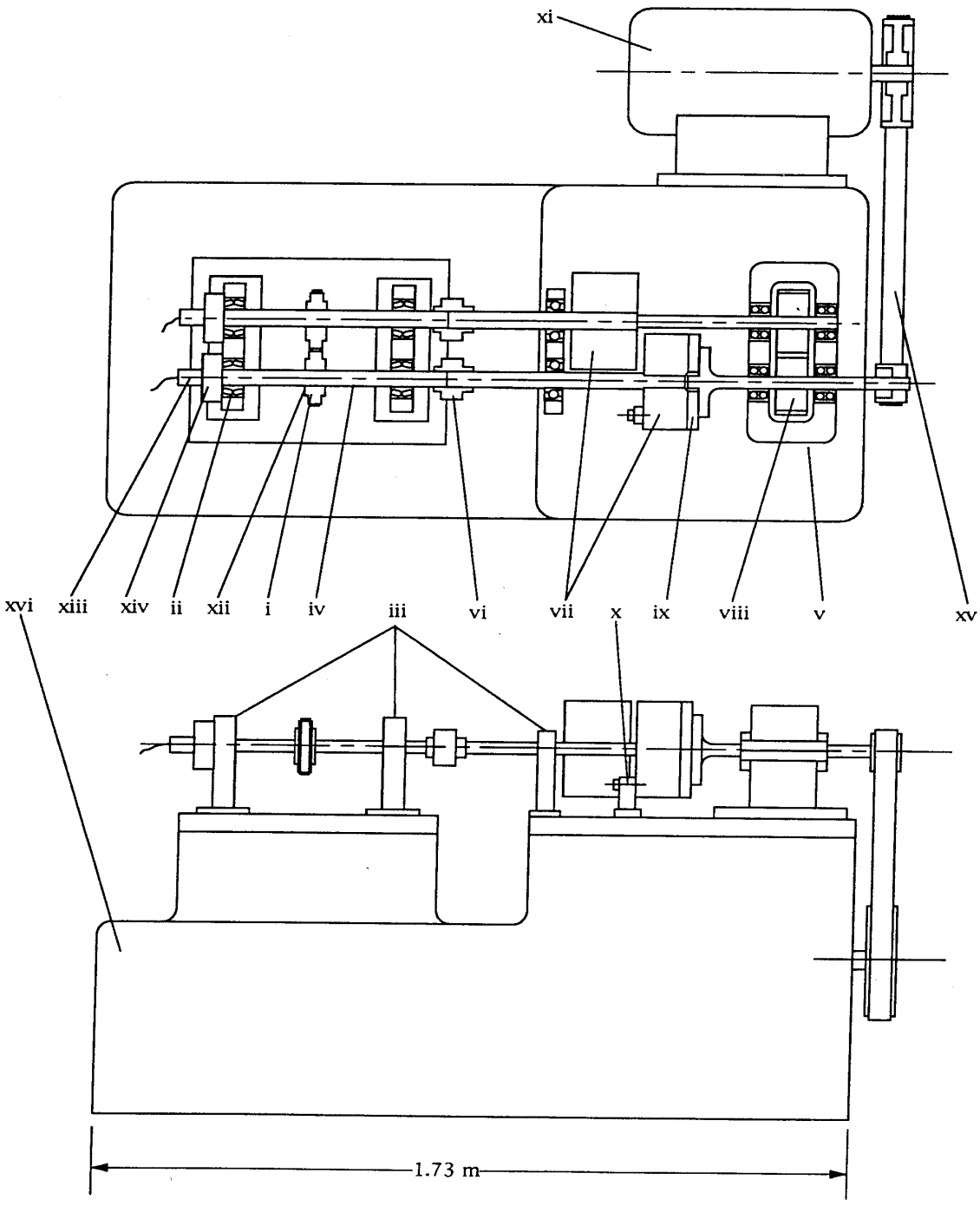

Figure 3.9 Schematic view of gear dynamic test machine.

Table 3.3

System parameters of the Gear Dynamic Test Machine

Diameter of test gears	$0.150\ m$
Number of teeth of test gears	35
Diameter of reaction gears	$0.150\ m$
Number of teeth of reaction gears	35
Test gear mesh stiffness	$2.5\times10^{8}\ N/m$
Reaction gear mesh stiffness	$5.0\times10^{8}\ N/m$
Mass of test gears	$2.2\ kg$
Mass of reaction gears	$4.4\ kg$
Polar moment of inertia of test gears	$1.4\times10^{-2}\ kg-m^{2}$
Polar moment of inertia of reaction gears	$2.8\times10^{-2}\ kg-m^{2}$
Diameter of Shaft 1	$0.040\ m$
Diameter of Shaft 2	$0.040\ m$
Polar moment of inertia of inertia element in Shaft 1	$3.8\times10^{-1}\ kg-m^{2}$
Mass of the inertia element in Shaft 1	$25\ kg$
Polar moment of inertia of inertia element in Shaft 2	$3.8\times10^{-1}\ kg-m^{2}$
Mass of inertia element in Shaft 2	$25\ kg$

are given in Figure 3.10. The system reaches the resonance peaks at 3000 and 3900 rpm as shown in Figure 3.10. For investigation of force and vibration transmissibility, first consider transmission error harmonic amplitudes in test side $\tilde{e}_{t1} = 0.0\,\mu m$ and in reaction side $\tilde{e}_{r1} = 1.0\,\mu m$. As shown in Figure 3.11, it is seen that there is no dynamic gear mesh forces experienced at the test side, which indicates excellent isolation characteristics. Similarly, in Figure 3.12 for $\tilde{e}_{t1} = 1.0\,\mu m$ and $\tilde{e}_{r1} = 0.0\,\mu m$, there is no reaction gear mesh force due to the test gear excitation confirming the same conclusion.

In Figure 3.13, the mode shapes at 0, 18, 59, 228, 1779 and 2267 *Hz* are shown. In Figure 3.13 (a-d) the gears rotate by same amounts in opposite directions, hence, there is no relative gear mesh displacement occurring at these modes. Therefore these modes do not cause any resonance peaks on the forced response. In Figure 3.13(e) test gears rotate in the same direction, which result in relative displacement on the test gear mesh. Similarly, the mode shape shown in Figure 3.13(f) reveals relative gear mesh displacements at the reaction gear mesh. As a result, these two modes are excited by the transmission error excitation.

3.3 NASA Gear Durability Test Machine

As the last example, NASA gear durability test machine [8-11] as shown in Figure 1.2 will be considered. It is composed of two relatively rigid parallel shafts connecting a wide facewidth reaction gear to a very compliant test gear pair. Here, there is no significant inertia element in between and shafts are rather short to cause any flexural vibrations. Therefore, a 4-DOF model is sufficient, which can be obtained from the

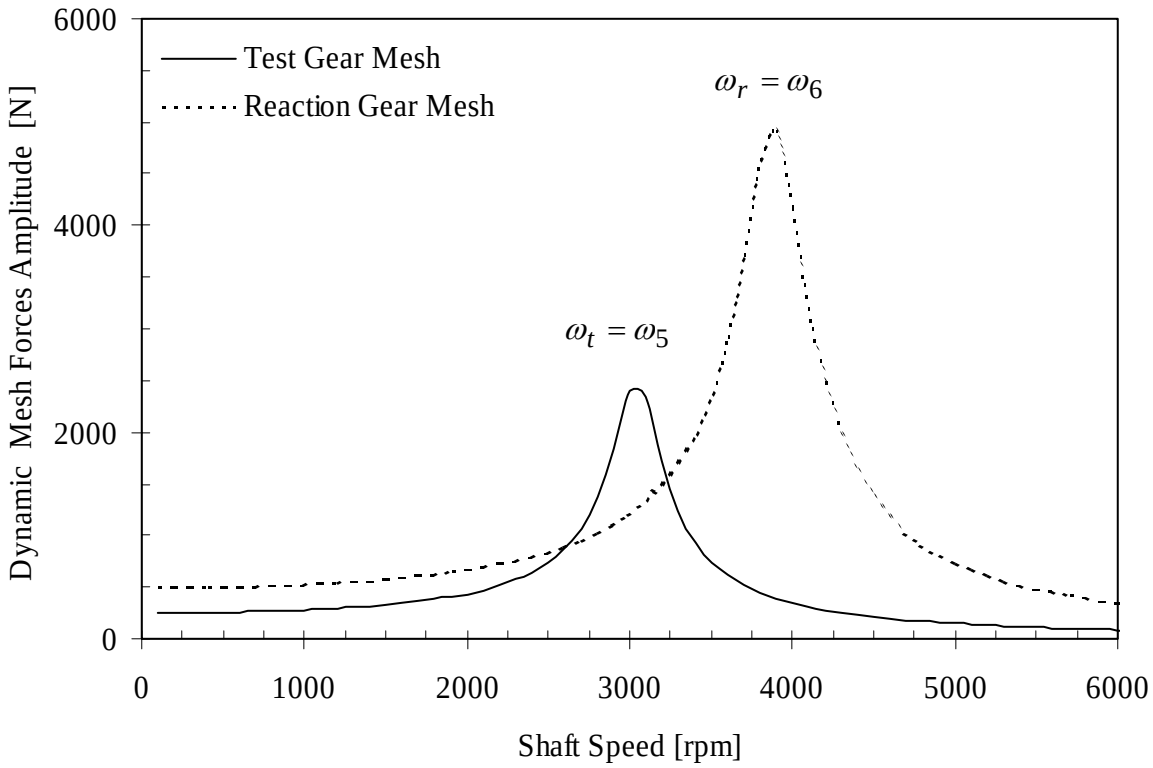

Figure 3.10 Dynamic mesh force amplitude of the test and reaction gear pair of gear dynamic test machine due to $\tilde{e}_{t1} = 1.0\,\mu m$ and $\tilde{e}_{r1} = 1.0\,\mu m$.

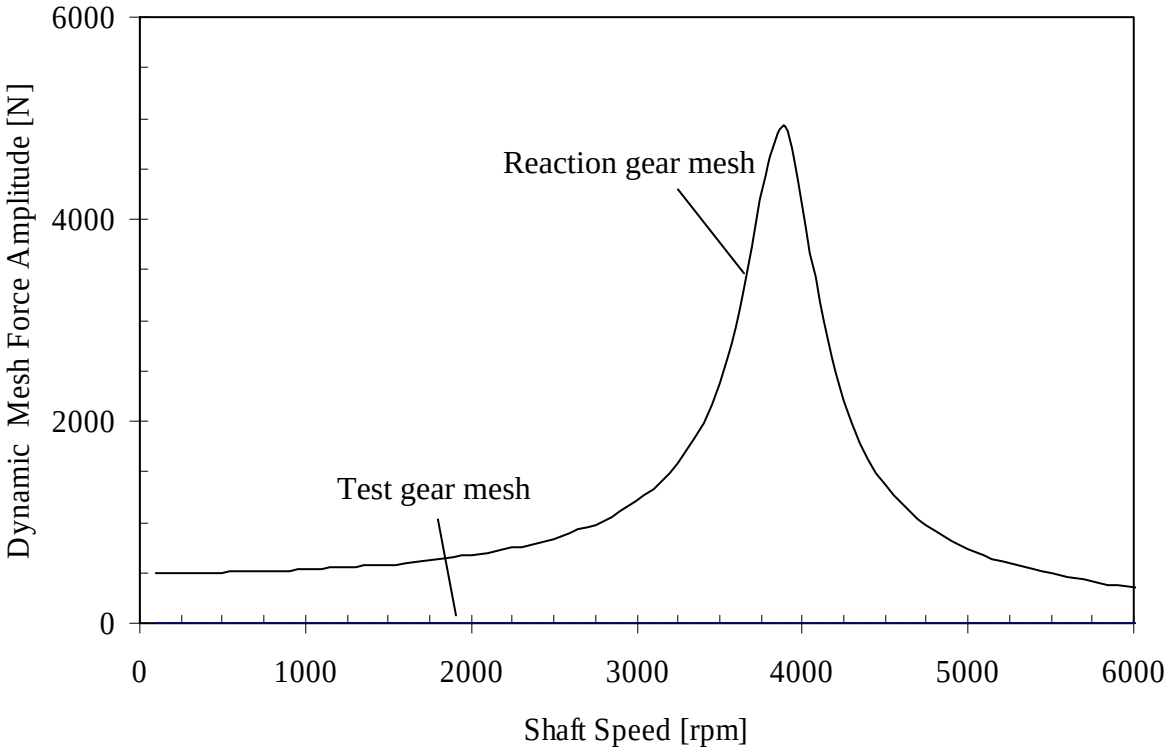

Figure 3.11 Dynamic mesh force amplitude of the test and reaction gear pairs of gear dynamic test machine due to $\tilde{e}_{t1} = 0.0\ \mu m$ and $\tilde{e}_{r1} = 1.0\ \mu m$.

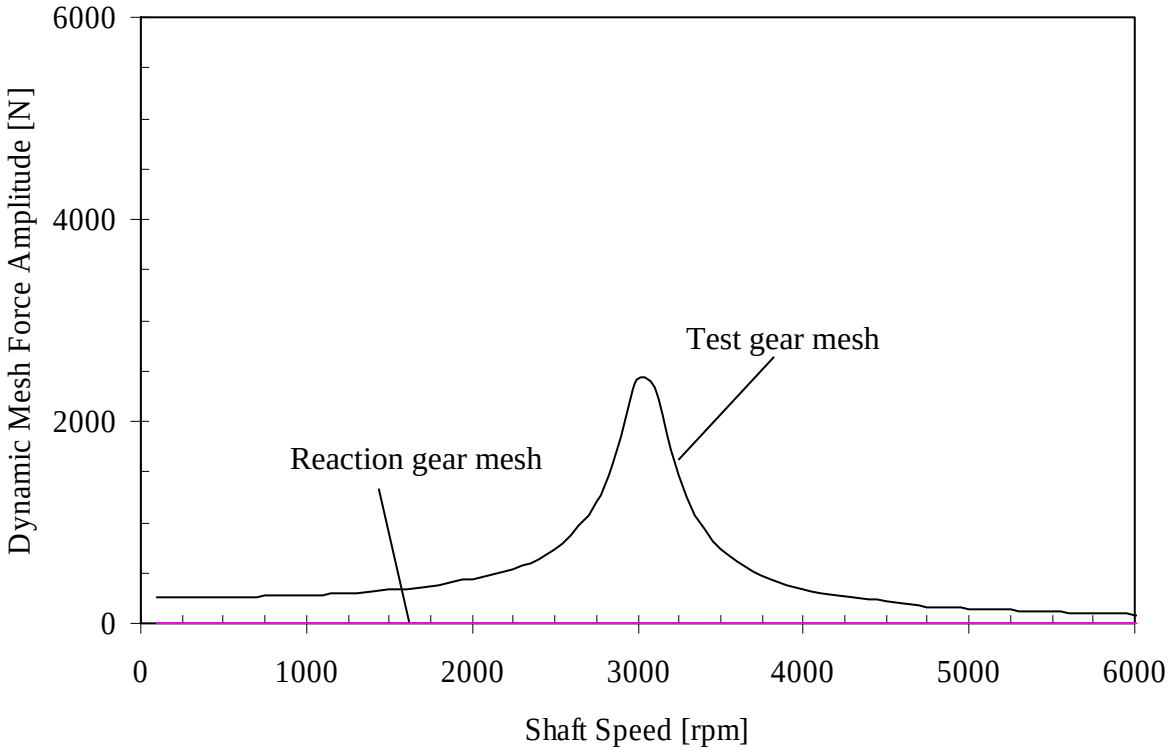

Figure 3.12 Dynamic mesh force amplitude of the test and reaction gear pairs of dynamic test machine due to $\tilde{e}_{t1} = 1.0\,\mu m$ and $\tilde{e}_{r1} = 0.0\,\mu m$.

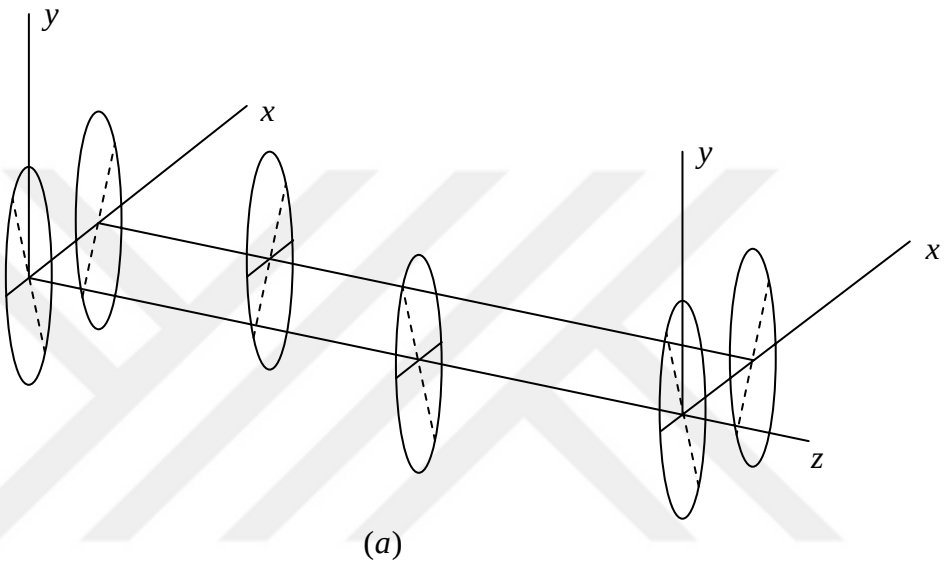

Figure 3.13 Mode shapes of dynamic gear test machine at (a) 0, (b) 18, (c) 59, (d) 228, (e) 1779 and (f) 2008 Hz.

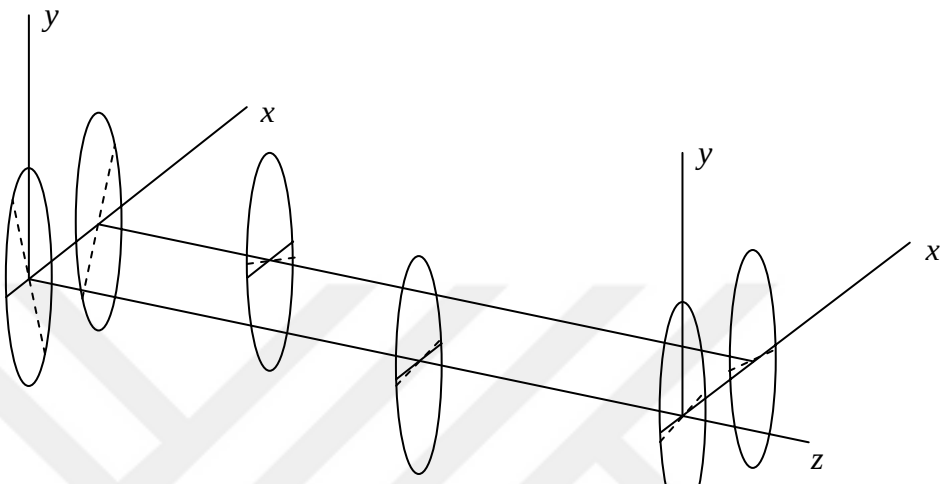

(*b*)

Figure 3.13 Continued.

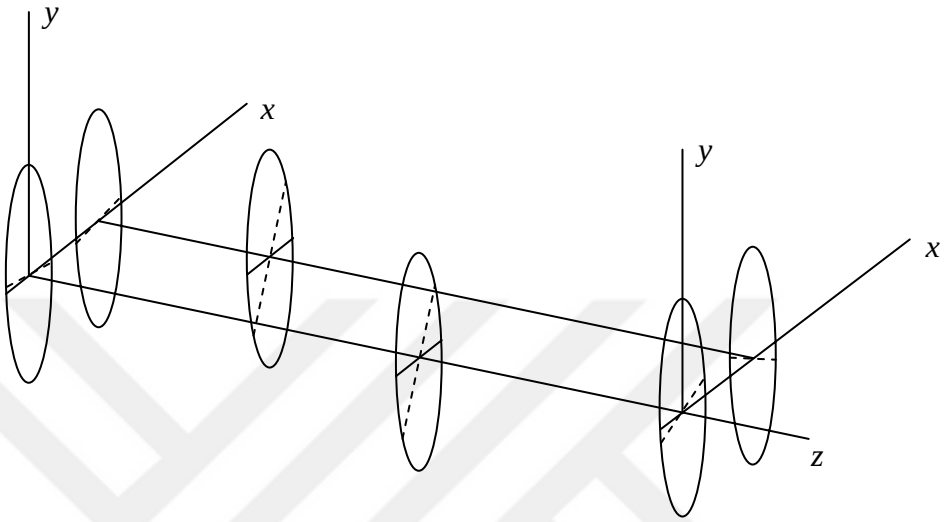

(*c*)

Figure 3.13 Continued.

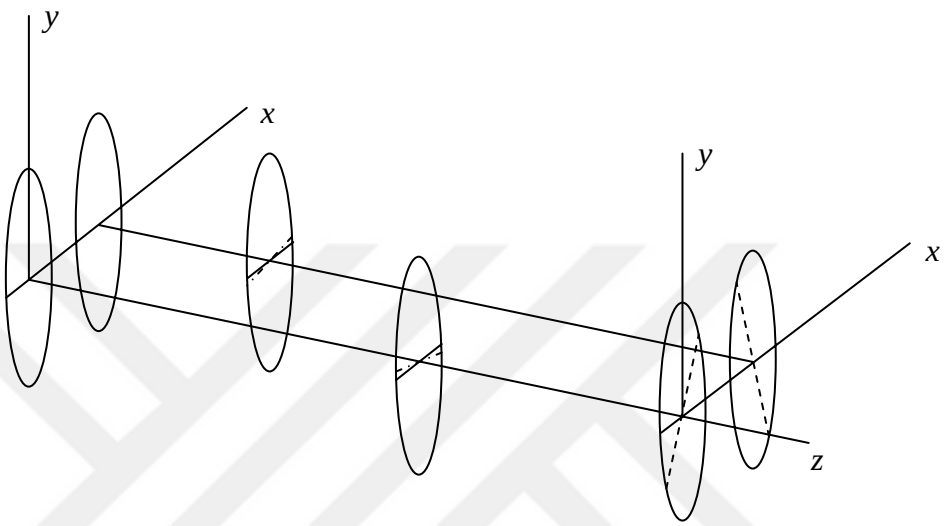

(*d*)

Figure 3.13 Continued.

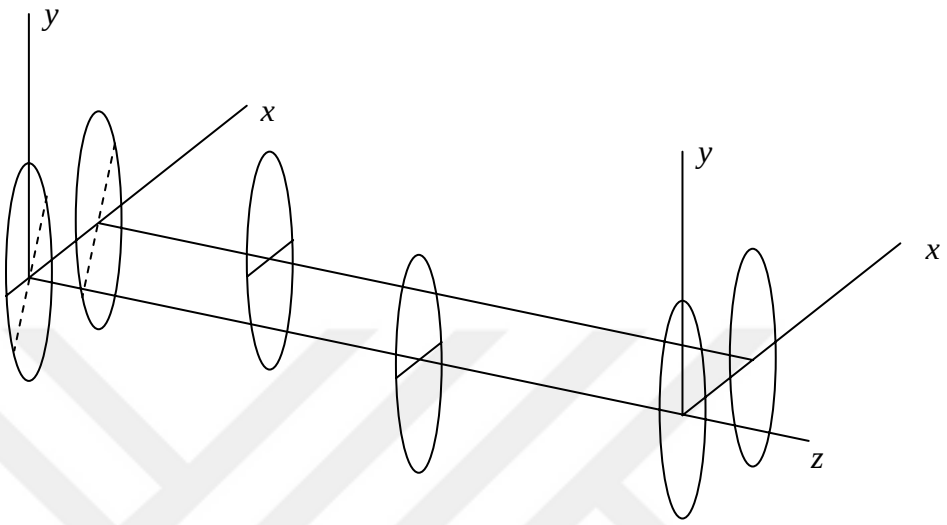

(*e*)

Figure 3.13 Continued.

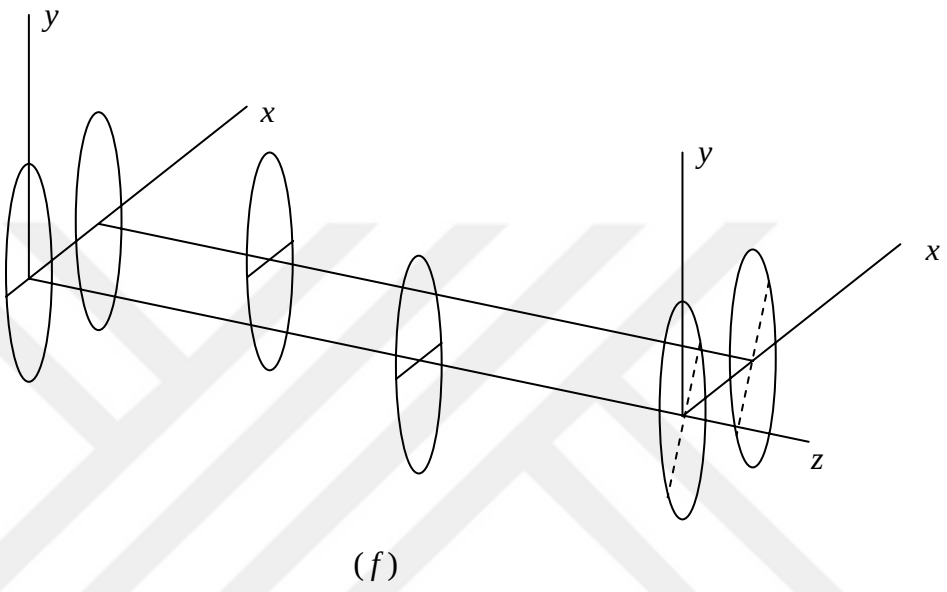

Figure 3.13 Continued.

6-DOF model by simply taking the flywheel inertias as $J_{f1} = 0$ and $J_{f2} = 0$. In Table 3.4, system parameters of this machine are listed. Again the force and vibration isolation issue is the main focus here. First, the transmission error harmonic amplitudes are taken as $\tilde{e}_{t1} = 1.0\,\mu m$ and $\tilde{e}_{r1} = 1.0\,\mu m$. A 5 percent of damping coefficient value is used for the analysis. Gear mesh stiffness values are estimated to be $\bar{k}_t = 8.6 \times 10^7\ N/m$ and $\bar{k}_r = 6.2 \times 10^8\ N/m$ for the test and reaction gear meshes, respectively. Dynamic gear mesh force amplitudes in the Figure 3.14. The resonance peaks appear at 8000, 8700, 10000 and 11000 rpm. These resonance peaks occur when $\omega_t = \omega_3$, $\omega_t = \omega_4$, $\omega_r = \omega_3$ and $\omega_r = \omega_4$.

For investigation of isolation issue, first consider the case when $\tilde{e}_{t1} = 0.0\,\mu m$ and $\tilde{e}_{r1} = 1.0\ \mu m$. Figure 3.15 shows dynamic gear mesh force amplitudes for this case. This figure suggests that the isolation between the test and reaction sides is not very good as large dynamic load amplitudes at the test side were obtained from the disturbances originated at reaction side. Figure 3.16 for $\tilde{e}_{t1} = 1.0\ \mu m$ and $\tilde{e}_{r1} = 0.0\ \mu m$ also supports the same conclusion. Looking at the mode shapes shown in Figure 3.17, first two modes at 0 and $2531\,Hz$ result in no relative gear mesh displacements, and hence, they are not excited. Meanwhile the last two modes in Figure 3.17, have non-zero relative gear mesh motions resulting in the resonance peaks shown in Figures 3.14 to 16.

Table 3.4

System parameters of the NASA gear durability test machine.

Diameter of test gears	0.089 m
Number of teeth of test gears	28
Diameter of reaction gears	0.089 m
Number of teeth of reaction gears	35
Test gear mesh stiffness	$8.6\times10^{7}\ N/m$
Reaction gear mesh stiffness	$6.2\times10^{8}\ N/m$
Mass of test gears	0.5 kg
Mass of reaction gears	3.0 kg
Polar moment of inertia of test gears	$3.6\times10^{-4}\ kg-m^{2}$
Polar moment of inertia of reaction gears	$2.8\times10^{-3}\ kg-m^{2}$
Diameter of Shaft 1 segments	0.030 , 0.035 , and 0.039 m
Diameter of Shaft 2 segments	0.030 , 0.035 , and 0.039 m

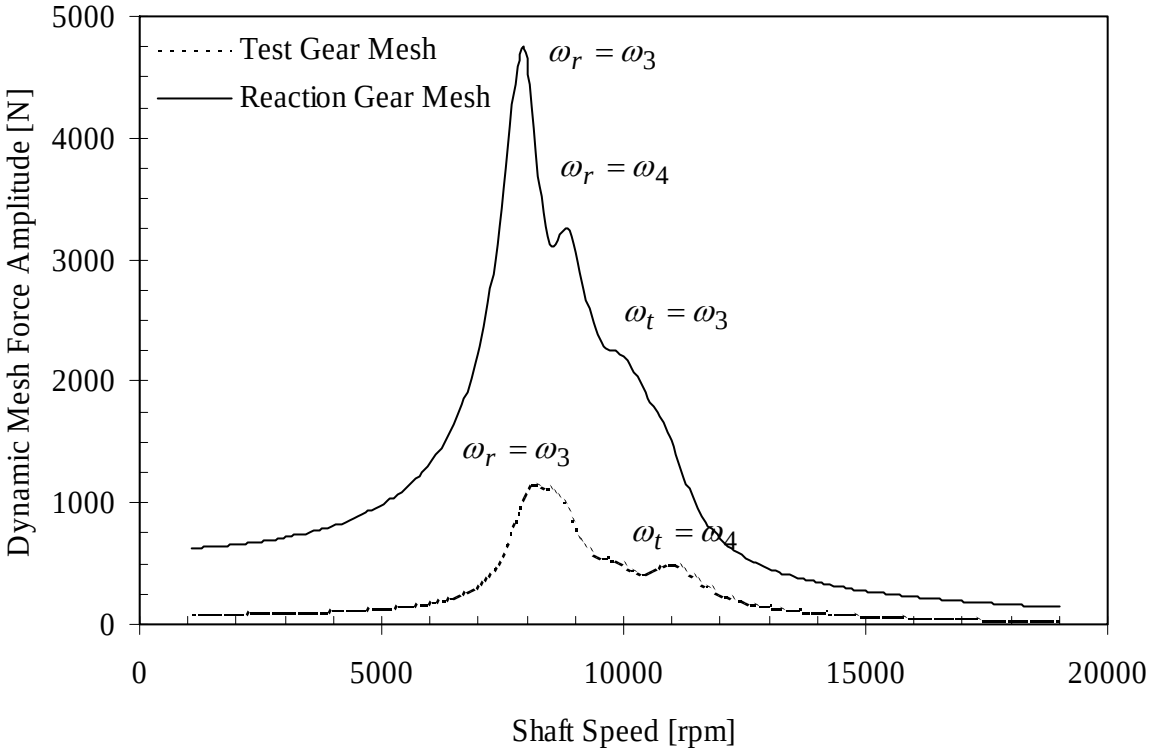

Figure 3.14 Dynamic mesh force amplitude of the test and reaction gear pairs of NASA gear durability test machine due to $\tilde{e}_{r1} = 1.0\ \mu m$ and $\tilde{e}_{t1} = 1.0\ \mu m$.

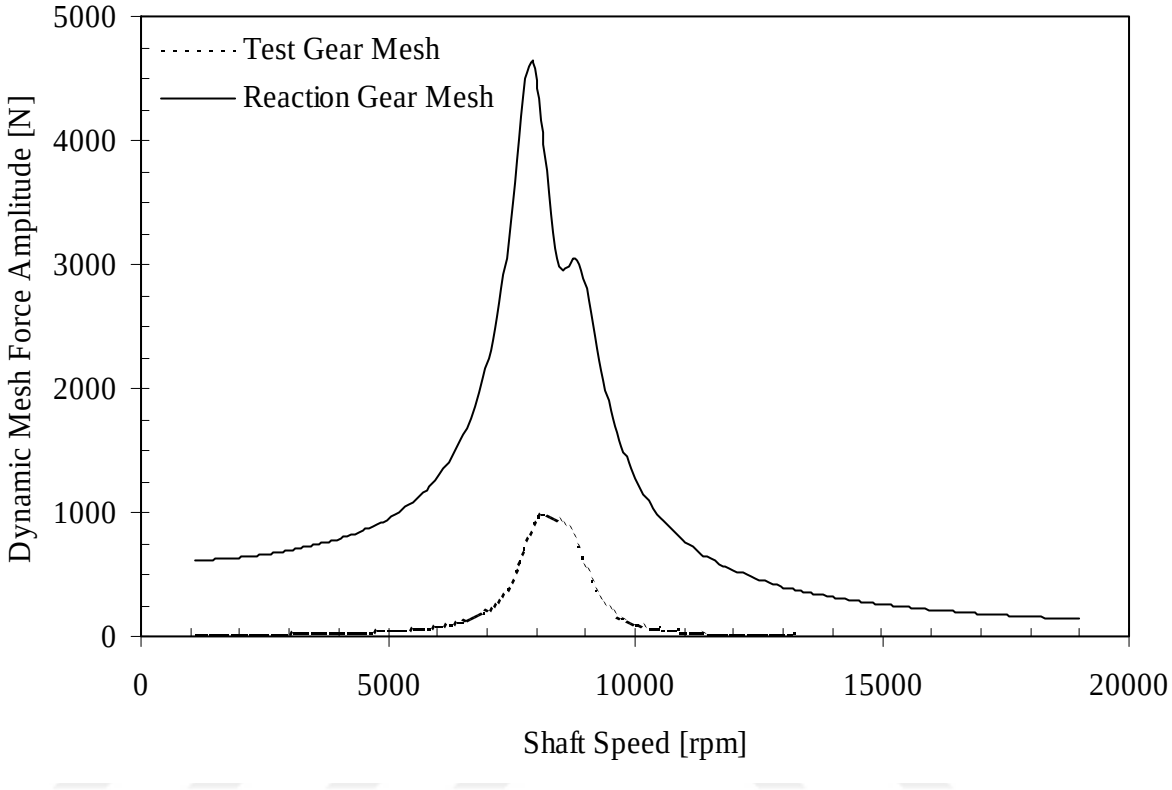

Figure 3.15 Dynamic mesh force amplitude of the test and reaction gear pairs of NASA gear durability test machine due to $\tilde{e}_{r1} = 1.0\ \mu m$ and $\tilde{e}_{t1} = 0.0\ \mu m$.

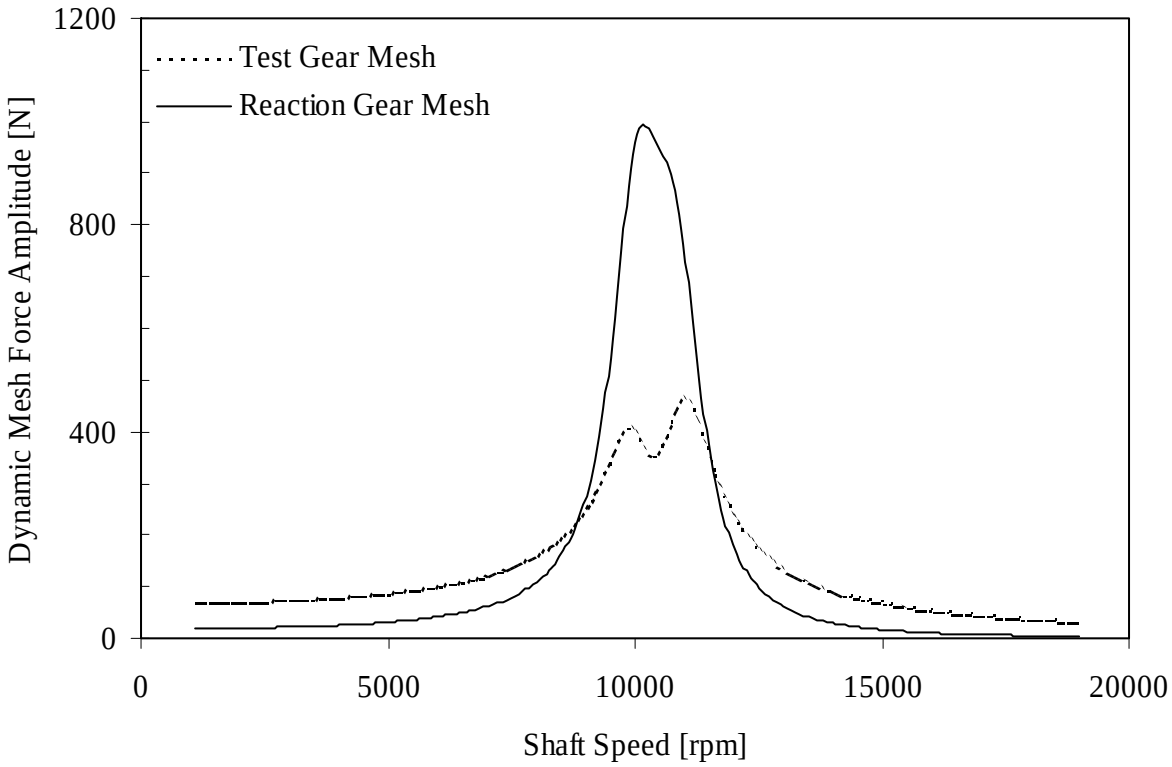

Figure 3.16 Dynamic mesh force amplitude of the test and reaction gear pair of NASA gear durability test machine due to $\tilde{e}_{r1} = 0.0\ \mu m$ and $\tilde{e}_{t1} = 1.0\ \mu m$.

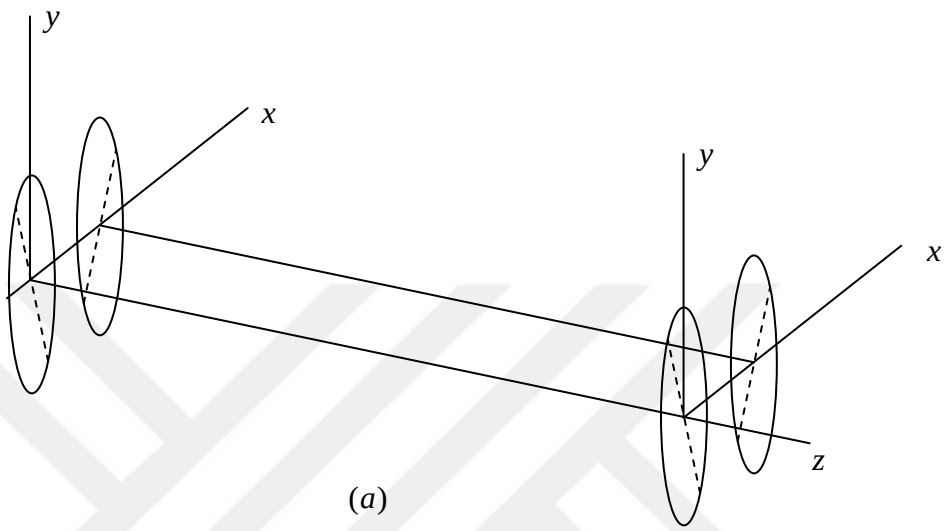

Figure 3.17 Mode shapes of NASA gear durability test machine at (a) 0, (b) 2531, (c) 4646 and (d) 5121 Hz.

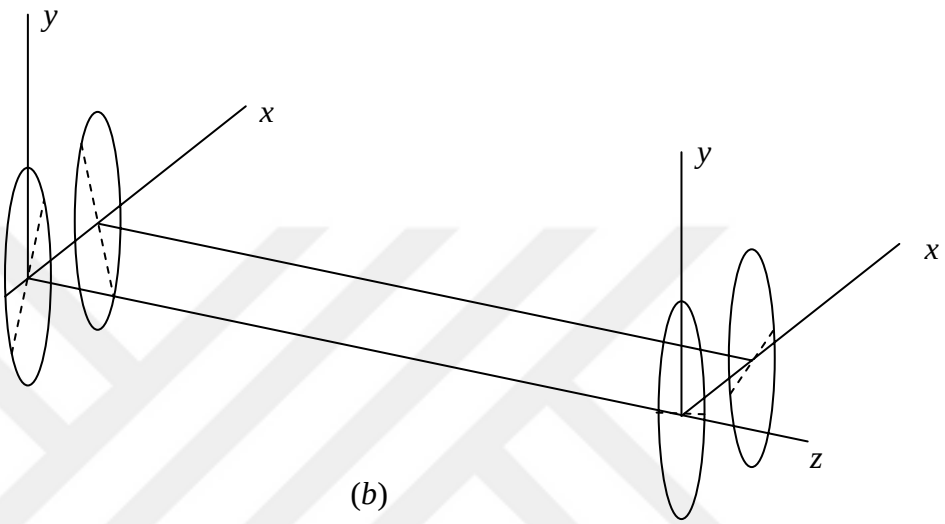

Figure 3.17 Continued.

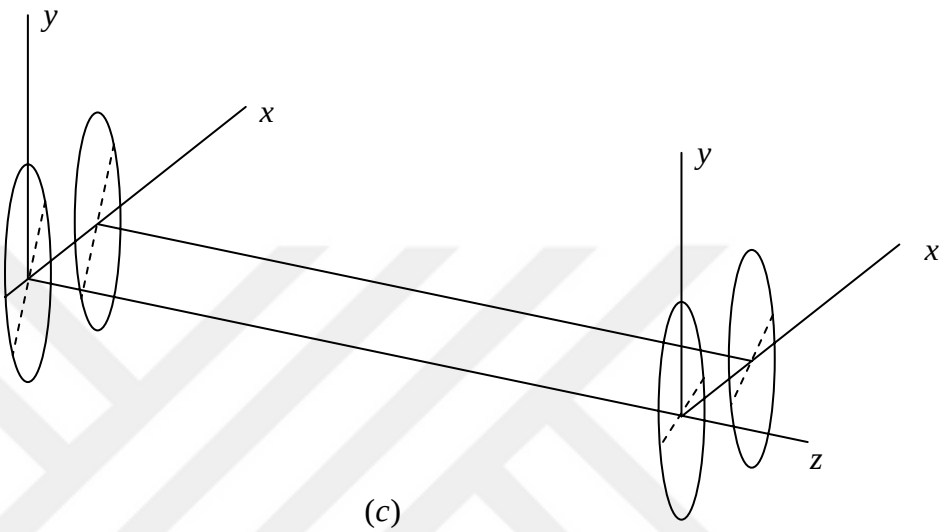

(*c*)

Figure 3.17 Continued.

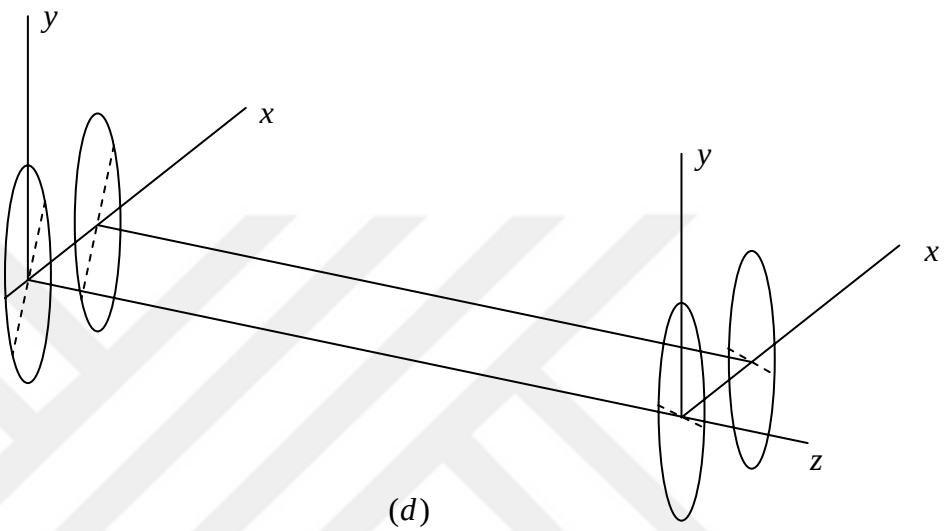

(*d*)

Figure 3.17 Continued.

CHAPTER 4

DESIGN GUIDELIINES

4.1 Derivation

As the results from Chapter 3 indicated, increasing the torsional flexibility of the connecting shafts improves vibration isolation characteristics of a four-square test machine significantly. The practical design question then becomes how much flexibility is enough for a good isolation. In an attempt design guidelines, the 4-DOF version of 6-DOF dynamic model shown in Figure 2.3 is considered here with $J_{f1} = J_{f2} = 0$. Combined shaft stiffness are given as

$$\hat{k}_{si} = \left[\frac{1}{k_{si}} + \frac{1}{\gamma_i k_{si}} \right]^{-1} \quad i = 1, 2. \tag{4.1}$$

The undamped equations of motion of the 4-DOF system is written in matrix form as

$$\mathbf{M}\ddot{\mathbf{q}}(t) + \mathbf{K}\mathbf{q}(t) = \mathbf{F}(t) \tag{4.2a}$$

$$\mathbf{M} = \begin{bmatrix} J_{t1} & 0 & 0 & 0 \\ 0 & J_{t2} & 0 & 0 \\ 0 & 0 & J_{r2} & 0 \\ 0 & 0 & 0 & J_{r1} \end{bmatrix} \tag{4.2b}$$

$$\mathbf{K} = \begin{bmatrix} r_{t1}^2 \bar{k}_t + k_{s1} & r_{t1} r_{t2} \bar{k}_t & 0 & -k_{s1} \\ r_{t1} r_{t2} \bar{k}_t & r_{t2}^2 \bar{k}_t + k_{s2} & -k_{s2} & 0 \\ 0 & -k_{s2} & r_{r2}^2 \bar{k}_r + k_{s2} & r_{r1} r_{r2} \bar{k}_r \\ -k_{s1} & 0 & r_{r1} r_{r2} \bar{k}_r & r_{r1}^2 \bar{k}_t + k_{s1} \end{bmatrix} \tag{4.2c}$$

Test gear pair is completely uncoupled from reaction gear pairs when $(k_{si} \to 0)$ $i = 1, 2.$ In this case two uncoupled gear pairs are obtained each having a zero and a nonzero natural frequency. In terms of the natural frequencies of the 4-DOF system given $\hat{k}_{si} \to 0$:

$\omega_1 \to 0$

$\omega_2 \to 0$

$\omega_3 \to \omega_t$

$\omega_4 \to \omega_r$

Here, the case when shaft 1 and shaft 2 assemblies are identical is considered:

$$r_{t1} = r_{t2} = r_{r1} = r_{r2} = r \tag{4.3a}$$

$$\hat{k}_{s1} = \hat{k}_{s2} = \hat{k}_s \tag{4.3b}$$

$$J_{t1} = J_{t2} = J_t \tag{4.3c}$$

$$J_{r1} = J_{r2} = J_r \tag{4.3d}$$

In this case uncoupled natural frequencies of each gear pairs are

$$\omega_t = \sqrt{\frac{\bar{k}_t}{m_{t_{eq}}}} = \sqrt{\frac{2r^2\bar{k}_t}{J_t}}, \quad m_{t_{eq}} = \frac{J_t}{2r^2} \tag{4.4}$$

$$\omega_r = \sqrt{\frac{\bar{k}_r}{m_{r_{eq}}}} = \sqrt{\frac{2r^2\bar{k}_r}{J_r}}, \quad m_{r_{eq}} = \frac{J_r}{2r^2} \tag{4.5}$$

and the stiffness matrix reduces to

$$[K] = \begin{bmatrix} r^2\bar{k}_t + \hat{k}_s & r^2\bar{k}_t & 0 & -\hat{k}_s \\ r^2\bar{k}_t & r^2\bar{k}_t + \hat{k}_s & -\hat{k}_s & 0 \\ 0 & -\hat{k}_s & r^2\bar{k}_r + \hat{k}_s & r^2\bar{k}_r \\ -\hat{k}_s & 0 & r^2\bar{k}_r & r^2\bar{k}_r + \hat{k}_s \end{bmatrix} \tag{4.6}$$

Defining the following dimensionless parameters

$$m_{r_{eq}} = \alpha^2 m_{t_{eq}}, \tag{4.7}$$

$$\kappa^2 = \frac{\bar{k}_r}{\bar{k}_t}, \tag{4.8}$$

$$\tilde{k}_t = r^2 \bar{k}_t, \quad \tilde{k}_r = r^2 \bar{k}_r \ , \tag{4.9}$$

$$\beta = \frac{k_s}{\tilde{k}_t}, \tag{4.10}$$

the stiffness matrix becomes

$$[K] = \begin{bmatrix} \tilde{k}_t + \hat{k}_s & \tilde{k}_t & 0 & -\hat{k}_s \\ \tilde{k}_t & \tilde{k}_t + \hat{k}_s & -\hat{k}_s & 0 \\ 0 & -\hat{k}_s & \tilde{k}_r + \hat{k}_s & \tilde{k}_r \\ -\hat{k}_s & 0 & \tilde{k}_r & \tilde{k}_r + \hat{k}_s \end{bmatrix} \tag{4.11}$$

By using (4.2b) and (4.11), characteristic determinant $\left|[K] - \omega^2[M]\right| = 0$ can be written as

$$\begin{vmatrix} \tilde{k}_t + \hat{k}_s - \omega^2 J_t & \tilde{k}_t & 0 & -\hat{k}_s \\ \tilde{k}_t & \tilde{k}_t + \hat{k}_s - \omega^2 J_t & -\hat{k}_s & 0 \\ 0 & -\hat{k}_s & \tilde{k}_r + \hat{k}_s - \omega^2 J_r & \tilde{k}_r \\ -\hat{k}_s & 0 & \tilde{k}_r & \tilde{k}_r + \hat{k}_s - \omega^2 J_r \end{vmatrix} = 0 \tag{4.12}$$

By dividing equation (4.12) by J_t and noting the following quantities

$$\frac{\tilde{k}_t}{J_t} = \frac{{\omega_t}^2}{2} \ , \ \alpha^2 = \frac{J_r}{J_t} \tag{4.14a,b}$$

$$\frac{k_s}{J_t} = \beta \frac{\omega_t^{\,2}}{2}, \quad \frac{k_r}{J_t} = \kappa^2 \frac{\omega_t^{\,2}}{2} \tag{4.14c,d}$$

the characteristic determinant becomes

$$\begin{vmatrix} \frac{\omega_t^2}{2}+\beta\frac{\omega_t^2}{2}-\omega^2 & \frac{\omega_t^2}{2} & 0 & -\beta\frac{\omega_t^2}{2} \\ \frac{\omega_t^2}{2} & \frac{\omega_t^2}{2}+\beta\frac{\omega_t^2}{2}-\omega^2 & -\beta\frac{\omega_t^2}{2} & 0 \\ 0 & -\beta\frac{\omega_t^2}{2} & \kappa^2\frac{\omega_t^2}{2}+\beta\frac{\omega_t^2}{2}-\omega^2\alpha^2 & \kappa^2\frac{\omega_t^2}{2} \\ -\beta\frac{\omega_t^2}{2} & 0 & \kappa^2\frac{\omega_t^2}{2} & \kappa^2\frac{\omega_t^2}{2}+\beta\frac{\omega_t^2}{2}-\omega^2\alpha^2 \end{vmatrix} = 0 \tag{4.15}$$

Solving equation (4.16) for ω yields the natural frequencies

$$\omega_1 = 0 \tag{4.16a-d}$$

$$\omega_2 = \left[\frac{1}{2}\frac{\beta(1+\alpha^2)}{\alpha^2}\right]^{1/2} \omega_t$$

$$\omega_3 = \left[\frac{1}{4}\frac{(\beta\alpha^2+\beta+2\alpha^2+2\kappa^2-\sqrt{\beta^2\alpha^4+2\beta\ \alpha^2+4\beta\alpha^4-4\beta\kappa^2\alpha^2+\beta^2-4\beta\alpha^2+4\kappa^2\beta+4\alpha^4-8\kappa^2\alpha^2+4\kappa^4}}{\alpha^2}\right]^{1/2} \omega_t$$

$$\omega_4 = \left[\frac{1}{4}\frac{(\beta\alpha^2+\beta+2\alpha^2+2\kappa^2+\sqrt{\beta^2\alpha^4+2\beta\ \alpha^2+4\beta\alpha^4-4\beta\kappa^2\alpha^2+\beta^2-4\beta\alpha^2+4\kappa^2\beta+4\alpha^4-8\kappa^2\alpha^2+4\kappa^4}}{\alpha^2}\right]^{1/2} \omega_t$$

In this form, the question to answer becomes what β value is required for a good isolation. For this purpose dynamic model is run for different β values to determine the

value for a good isolation. In Figure 4.1, isolation characteristics for $\beta = 1.0$, 0.5 and 0.1 are shown. It can be concluded from this figure that value around $\beta = 0.1$ results in good isolation.

Figure 4.2 shows the influence of β on ω_i ($i = 1$ to 4) for $\alpha = 2$ and $\kappa = 3$. Using $\beta = 0.1$ as a potential design limit for a good isolation one can conclude that $\omega_2 / \omega_t \leq 0.25$, $\omega_3 / \omega_t \leq 1.025$ and $\omega_4 / \omega_t \leq 1.5$. For any other parameters, ω_i ($i = 1$ to 4) can be calculated from equation (4.16) and compared to ω_t value to determine if the isolation characteristic are acceptable.

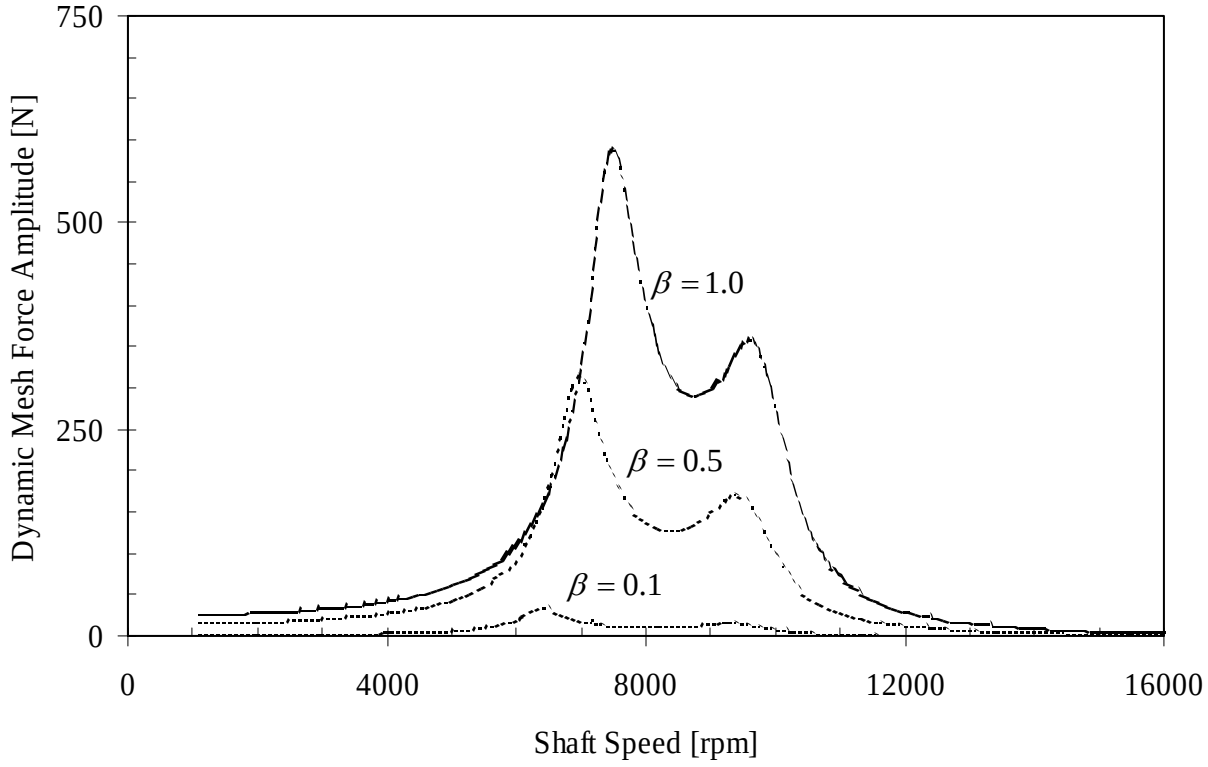

Figure 4.1. Comparison of test gear dynamic mesh force for a system having $\alpha = 2$, $\kappa = 3$ and $\beta = 1.0, 0.5$ and 0.1 due to $\tilde{e}_{t1} = 0.0\ \mu m$ and $\tilde{e}_{r1} = 1.0\ \mu m$.

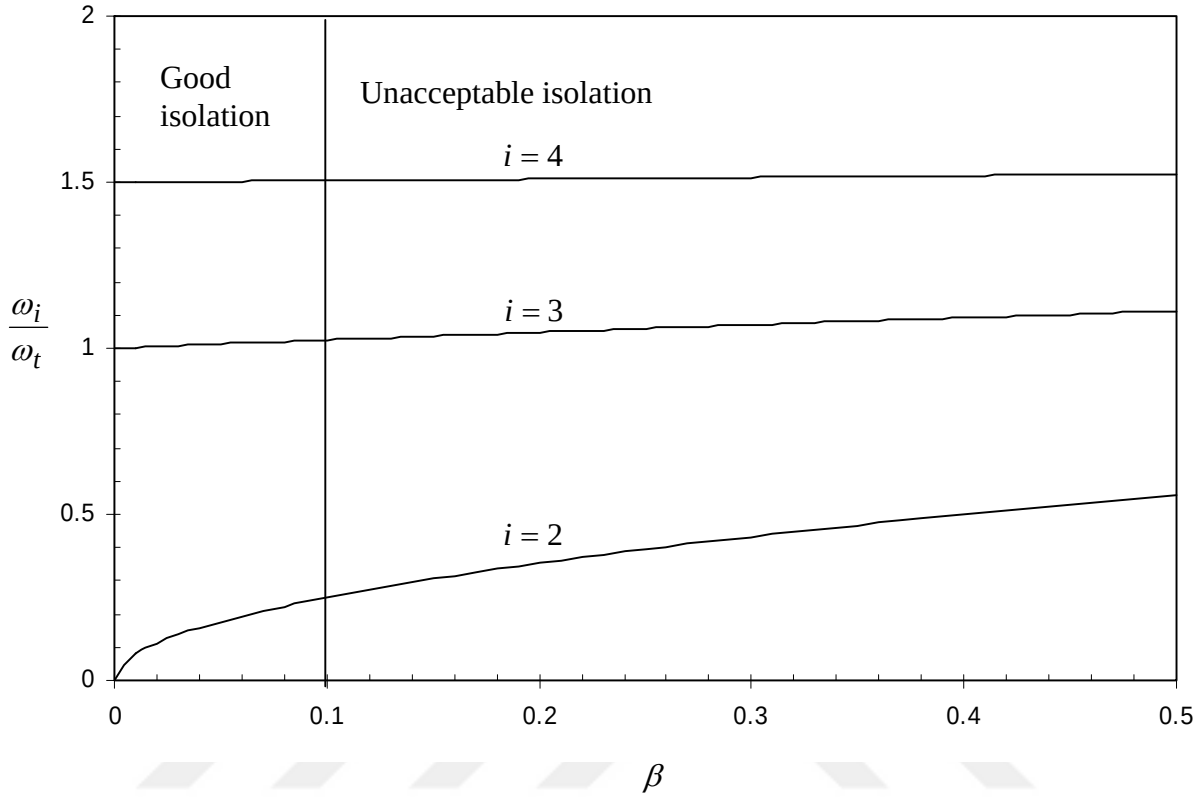

Figure 4.2 Variation of ω_i with β.

4.2 Summary and Conclusion

In this study, a three dimensional and purely torsional model were developed to investigate the dynamic behavior of four-square gear test machines, specifically the interaction between the test and reaction gear pars. The first model was based on three-dimensional finite elements of the flexible shafts connecting the test and reaction gearboxes. Three-dimensional stiffness models of helical gear pairs and rolling element bearings were used with the FE model of the shafts to find the free and forced vibration characteristics. The second model represented a limiting case when only torsional motions were allowed. The gear transmission errors and eccentricities were considered as the excitations for both models. Eigen Value solution and Modal Summation Technique were used to compute natural modes and forced response, respectively.

A number of gear dynamics and durability test machines were considered as the example cases. The interactions between the test and reaction gearboxes were investigated for each test machine to determine their force and vibration isolation capabilities. Results indicated that any added torsional flexibility or rigid inertia between the test and reaction gear sets helped improve the isolation of the test gear pair from the disturbances originated at the reaction gearbox. The comparison of 3D and torsional models indicated that, while 3D model is more accurate, the torsional model adds value in deriving simple design equations. Such equations can potentially be used for designing such machines with acceptable vibration isolation characteristics. With the help of these equations, a designer can select the required flexibility for the connecting shafts.

One of the important parameters in design of a four-square type machine having good isolation characteristics is the ratio of the shaft stiffness to the gear mesh stiffness, β. To achieve a good isolation of the test gearbox from the reaction side, β should be less than 0.1. In addition, adding flywheel inertias and elastic couplings between reaction and test gearboxes will improve isolation of test gearbox from reaction gearbox. Hence, the test results will be more reliable. Yet the designer must be careful in reducing shaft stiffness and adding flywheels can easily become a problem. The three-dimensional model can be used in such cases to assess and prevent such problems.

References

[1] Iida, H., Tamura, A., Kikuch, K., Agata, H., 1980, "Coupled Torsional-flexural Vibration of a Shaft in a Geared Systems of Rotors", *Bulletin of the JSME,* **186**, pp.2111-2117

[2] Iida, H., Tamura, A., Yamada, Y. , 1985, "Vibrational Characteristics of Friction Between Gear Teeth", *Bulletin of the JSME,* **241**, pp.1512-1519

[3] Umezawa, K., Sato, T., 1985, "Influence of Gear Error on Rotational Vibration of Power Transmission Spur Gear", *Bulletin of the JSME,* **246**, pp.3018-3024

[4] Umezawa, K., Sato, T., Houjoh, H., Suzuki, T., 1985, "Vibration of Power Transmission Helical Gears", *Bulletin of the JSME,* **238**, pp.694-700

[5] Umezawa, K., Houjoh, H., Maki, H., 1988, "Estimation of the Vibration of In-Service Gears by Monitoring the Exterior Vibration ", *JSME International Journal,* **3**, pp.588-592

[6] Choy, F. K., Ruan, Y. F., Zakrajsek, J. J., Oswald, F. B., Coy, J. J., 1991, "Analytical and Experimental Study of Vibrations in a Gear Transmission", *NASA technical memorandum,* **104434**, pp.1-20

[7] Liou, C. H., Lin H. H., Oswald, F. B., Townsend, D. P., 1991, "Effect of Contact Ratio on Spur Gear Dynamic Load", *International Power Transmission and Gearing Conference,* **De-Vol43-1**, pp.29-33

[8] Townsend, D. P., Zaretsky, E. V., 1974, "A Life Study of AISI M-50 and Super Nitralloy Spur Gears With and Without the Tip Relief", *Journal of Lubrication Technology,* **73**, pp.583-590

[9] Townsend, D. P., Bamberger, E. N., Zaretsky, E. V., 1976, "A Life Study of Ausforged Standard forged, and Standard Machined AISI M-50 Spur Gears", *Journal of Lubrication Technology* , **73**, pp.418-425

[10] Townsend, D. P., Akin, L. S., 1981, "Analytical and Experimantal Spur Gear Tooth Temperature as Affected by Operating Variables", *Journal of Mechanical Design* , **80**, pp.219-226

[11] Townsend, D. P., Shimski, J., 1991, "Effect of Two Synthetic Lubricants on Life of AISI 9310 Spur Gears", *NASA Technical Memorandum* , **104352**, pp.1-14

[12] Yoshida, A., Fujita, K., Miyanishi, K., Torii, O., Fujita, Y., Konishi, D., 1987, "A Study on the Effect of Tooth Fatigue on the Dynamic Performance of a gear Pair", *JSME International Journal* , **265**

[13] Yamanaka, M., Kishi K., Inoue K., Kato M., Masuyama, T., Morikawa K., Nagahara M., 2000, "Evaluation of Pitting Life of Carburized Gears Lubricated by ATF and Traction Oil", *ASME 2000 Design Engineering Technical Conferences and Computers and Information in Engineering Conference* , **DETC2000/PTG-14374**, pp.1-14

[14] Dahmen, C., Schonwerth, O., 1991, "A Realistic, Function-Oriented Oil Test", *The Volvo WZL Pittingtest,* pp.2173-2185

[15] Schaller K. V., A., Michaleis K., 1991, "Betriebsfestingkeitsuntersuchungen zur Grubchenbildung an Einsatzgeharteten Strinradflanken", *Forschungsheft Forschungvereinigung Antriebstechnik E.V.,* **125/II**, pp.1-150

[16] Harris S. L., 1958, "Dynamic Loads on the teeth of spur gears", M. A., A.M.I.C.E pp.88-112

[17] Munro R. G., 1962, *The Dynamic Behavior of Spur Gears,* PhD Dissertation, University of Cambridge.

[18] Munro, R. G., Yildirim, N., 1994, "Some measurements of Static and Dynamic Transmission Errors of Spur Gears, *Proceeding of International Gearing Conference,* New Castle, UK, pp.371-376

[19] Utagawa, M., Harada, T., 1961, "Dynamic Loads on Spur Gear Teeth at High Speed", *Bulletin of JSME,* Vol.4, **16**

[20] Gregory, R. W., Harris S. L., Munro, R.G., 1963, "Dynamic Behavior of Spur Gears", *Proc Institution of Mechanical Engineers,* Vol.178, **8,** pp.207-226

[21] Nakamura, K., 1967, "Experimental Studies about the Effect of Dynamic Loads upon Gear Noises", *Bulletin of JSME,* Vol.10, **37,** pp.180-188

[22] Seager, D. L., 1968, "Dynamic Behavior of Helical Gears", *ASME Journal,* **69-Vibr-16,** pp.1-5

[23] Remmers, E. P., 1971, "The Dynamics Gear Pair Systems", *ASME Journal,* pp.1-7

[24] Ichimaru, K., Hirano F., 1972, "Dynamics Behavior of Heavy-Loaded Spur Gears", *ASME Journal,* **72-PTG-14**, pp.1-7

[25] Kiyono, S., Aida, T., Fujii, Y.,1978, "Vibration of Helical Gears", *Bulletin of the JSME,* Vol.21, **155**, pp.923-931

[26] Kahraman, A., Singh, R., 1991, "Interaction Between Time-Varying Mesh Stiffness and Clearance Non-Linearities in a Gear System.", *Journal of Sound and Vibration,* **146**, pp.135-156

[27] Kahraman, A., 1992, "On the Response of a Preloaded Mechanical Oscillator with Clearance: Period Doubling and Chaos", *Non-Linear Dynamics* , **3**, pp.183-198

[28] Kahraman, A., Blankenship, G. W.,1995, "Steady State Forced Response of a Mechanical Oscillator with Combined Parametric Excitation and Clearance Type Non-Linearity", *Journal of Sound and Vibration,* **185**, pp.743-765

[29] Kahraman, A., Blankenship, G. W.,1996, "Interactions Between Commensurate Parametric and Forcing Excitations in a System with Clearance", *Journal of Sound and Vibration,* **194**, pp.317-336

[30] Kahraman, A., Blankenship, G. W.,1997, "Experiments on Non-Linear Dynamic Behavior of an Oscillator with Clearance and Periodically Time-Varying Parameters", *Journal of Applied Mechanics,*Vol.64, pp.217-226

[31] Wagaj P., Kahraman, A., 1997, "Impact of Tooth Profile Modifications on the Transmission Error Excitation of Helical Gear Pairs", *6th Biennial Conference on Engineering Systems Design and Analysis, Istanbul, Turkey,* **ESDA 2002/DES-005**, pp.1-11

[32] Kahraman, A., Ozguven, H. N., Houser, D. R., Zakrajsek, J. J., 1992, "Dynamic Analysis of Geared Rotors by Finite Elements," *ASME Journal of Mechanical Design*, **114**, pp. 507-514.

[33] Kubur, M., 2002, *Dynamic Analysis of a Multi-shaft Helical Gear Transmission by Finite Elements*, M.S. Thesis, The University of Toledo, Toledo, OH.

[34] Ozguven, H. N. and Ozkan, Z. L., 1983, "Whirl Speeds and Unbalance Response of Multi-Bearing Rotors Using Finite Elements," *ASME Journal of Vibration, Acoustics, Stress, and Reliability in Design*, **106**, pp. 72-79.

[35] Kahraman, A., 1993, “Effect of Axial Vibrations on the Dynamics of a Helical Gear Pair,” *ASME Journal of Vibration and Acoustics*, **115**, pp. 33-39.

[36] Lim, T. C. and Singh, R., 1990, “Vibration Transmission through Rolling Element Bearings, part I: Bearing Stiffness Formulation,” *Journal of Sound and Vibration*, **139**, pp. 179-199.

[37] Ewins, D. J., 1986, *Model Testing: Theory and Practice*, Research Studies Press, Hertfordshire, England.